Pergamon

Int. J. Solids Structures Vol. 34, No. 19, pp. 2357–2392, 1997

0020–7683/97 $17.00 + .00

PII: S0020–7683(96)00171–0

INDENTATION OF SOLIDS WITH GRADIENTS IN ELASTIC PROPERTIES: PART I. POINT FORCE

A. E. GIANNAKOPOULOS and S. SURESH†
Department of Materials Science and Engineering, Massachusetts Institute of Technology, Cambridge, MA 02139, U.S.A.

(*Received* 25 *January* 1996; *in revised form* 2 *August* 1996)

Abstract—Analytical and computational results are presented on the evolution of stresses and displacements due to indentation from a normal point force on an elastic substrate whose Young's modulus E varies as a function of depth, z, beneath the indented surface. With the exception of variation of properties with depth, the material is assumed to be linearly elastic and locally isotropic. Closed-form solutions are derived for several fixed values of the Poisson ratio, ν, and variations in E which follow two prescribed functions of z: (1) a simple power law, $E = E_0 z^k$, where $0 \leqslant k < 1$ is a non-dimensional exponent; (2) an exponential law, $E = E_0 e^{\alpha z}$, where E_0 is Young's modulus at the surface, $\alpha < 0$ denotes a hardened surface (e.g., graded ceramic coatings on metallic substrates) and $\alpha > 0$ denotes a soft surface (e.g., modulus variations measured as a function of depth beneath the earth's surface for solids and rocks). The analytical solutions are checked with detailed finite element simulations. It is shown that, for the power law case, there exists a critical Poisson ratio, ν_{cr}, above which drastic changes occur in the stress distribution under the point load. Finite element results reveal, however, that the response is relatively less sensitive to the variation of ν (on either side of ν_{cr}) than to the variation of E with depth. Applications of the present results are discussed, wherever appropriate, to surface treatments of engineering structures, thick coatings, thin-film multilayers for microelectronic devices, and settling of foundations in the context of soil mechanics and rock mechanics. © 1997 Elsevier Science Ltd.

1. INTRODUCTION

The stress and deformation fields in elastic solids subject to point loads have long been the subject of considerable research. Fundamental solutions for the evolution of stresses and displacements due to surface tractions in a homogeneous elastic half-space were presented by Boussinesq (1885) and Love (1927). Comprehensive reviews can be found in Gladwell (1980), Johnson (1985) and Hills *et al.* (1993).

A particular extension of this basic problem involves the study of indentation of compositionally graded materials by point forces and other loading geometries (e.g., punch, sphere, diamond pyramid indentor, etc.), and the penetration of geo-materials, such as soils and rocks, where the elastic properties vary as a function of depth beneath the surface. This topic has major applications in a wide variety of scientific and technological areas which include:

- the synthesis of advanced coatings for structural components to guard against thermal and tribological damage,
- the probing of the *local* physical and mechanical properties of composite materials by means of micro-indentation or nano-indentation with the objective of developing micromechanical models for deformation,
- the estimation of the fracture properties of materials for the purpose of ranking materials on the basis of their damage tolerance,
- structural porous materials with gradients in porosity, which are being considered as candidates for wings and fuselages of manned and unmanned aerospace vehicles,
- penetration of potential armor materials (with compositionally graded layers) by projectiles, and
- the development of geotechnical analyses for the settlement of foundations on deep deposits of soils, clay, and rocks.

† Author to whom correspondence should be addressed.

A number of current applications in engineering structural components, and micro- and opto-electronics involve compositionally graded materials (see, for example, Ilschner and Cherradi, 1994; Suresh and Needleman, 1996). Carburization and nitriding of steels on the surfaces of components subjected to repeated contact to impart enhancements in hardness result in a gradient in carbon and nitrogen concentration beneath the surface. Compositionally graded interfaces between metallic substrates and ceramic outer coatings are being explored by recourse to a variety of well-established processing methods for the purpose of minimizing internal stresses arising from thermal mismatch, improving the interfacial bond strength, suppressing the onset of plastic flow, reducing the deleterious effects of singularities at free edges, and increasing the thickness of ceramic coatings (e.g., Finot and Suresh, 1996). In thin-film semiconductor devices, graded interlayers are grown by such methods as molecular beam epitaxy or chemical vapor deposition for the purpose of controlling the population, distribution and kinetics of misfit and threading dislocations in heteroepitaxial structures (Fitzgerald *et al.*, 1992). An example is the thin-film trilayer system comprising a compositionally graded layer of $In_xGa_{1-x}As$ which is sandwiched between layers of $In_{0.12}Ga_{0.88}As$ and GaAs.

In geomechanics, the variation of the elastic properties of soils, sands, clay and rocks as a function of depth beneath the surface of the earth is known to have a strong effect on the settlement and stability of foundations and retaining walls and on plate tectonics. For example, there is experimental evidence which indicates that for soils, the values of Young's modulus (E) vary with depth below the surface (z) as $E = E_0 z^k$, where E_0 is the modulus of the homogeneous soil ($k = 0$) and $0 \leqslant k < 1$; $k = 1$ denotes the so-called "Gibson soil".

Despite the large number of diverse applications, few *general* solutions to the problem of indentation on compositionally graded elastic substrates have been attempted. Holl (1940), Hruban (1958) and Lekhniskii (1962) considered the specific case of deformation under a point load of an elastic half-space wherein the elastic modulus varies as a power-law function of depth from a value of zero at the indented surface. In that work, the radial stress fields were constructed for the particular critical Poisson ratio $\nu = \nu_{cr} = 1/(k+2)$. This critical value of ν comes as a requirement for the existence of radial stresses in the half space, i.e., for the principal stresses to be focused at the site of application of the point force. The general variation of the response due to point force for an arbitrary value of ν ($\neq \nu_{cr}$) has not been addressed thus far.

Gibson (1967), Gibson *et al.* (1971, 1975), Brown and Gibson (1972), Awojobi and Gibson (1973) and Calladine and Greenwood (1978) presented results for the displacement and stresses of linearly non-homogeneous deep elastic strata, with a primary focus on the settlement of foundations. Holl (1940) examined the power-law variation of Young's modulus, $E = E_0 z^k$, in the context of stress transmission in earth, for the particular case of $\nu = 1/(k+2)$. Note that the cases analyzed by Holl correspond to the incompressible homogeneous soil ($k = 0$, $\nu = 0.5$), and the Gibson soil ($k = 1, \nu = 1/3$). Mossakovski (1958) and Rostovtsev and Khranevskaia (1971) considered the deformation of an elastic substrate, with a power-law variation in Young's modulus under a compressive force produced by a punch and a point force, respectively. Several of these previous studies were incomplete or contained errors, and used particular values of the Poisson ratio.

Booker *et al.* (1985) studied the response of an elastic non-homogeneous half-space subject to line and point loads as well as circular and strip loads. The results of Booker *et al.* are specific to the case where the Poisson ratio of the substrate $\nu = 0.25$. A particular restriction of all of the foregoing studies is that they pertain only to specific choices of ν *which is assumed to be spatially invariant.* This assumption, as shown later in the present paper, can lead to incorrect descriptions of the stress and displacement fields in some cases.

The present work was undertaken with the objective of developing a fundamental understanding of the micromechanics of indentation of a compositionally graded elastic solid. Through a combination of analytical, computational and experimental investigations, this work seeks to examine the force-depth relations, the depth-contact radius relations, the radial distribution of contact pressure due to indentation, and other stress and deformation fields at the contacting surface due to a point force, a line force, as well as conical, spherical, and punch indentors. The results of this work will be discussed in a series of

related articles. This paper, Part I, presents the analytical and finite element results of the indentation of a compositionally graded elastic medium by a point force, where several different profiles of gradients in Young's modulus and Poisson ratio are considered to address a wide variety of engineering applications.

2. PROBLEM FORMULATION

The present problem is to develop solutions for the fields created by a point force, P, acting normally on the surface of a semi-infinite elastic solid, in the absence of body forces. The coordinate system is attached at the point application of the force with the usual conventions (shown in Figs 1 and 2). The material is assumed to be linearly elastic, inhomogeneous and locally isotropic within the context of small strains and small rotations. Within the elastic analysis, possible residual stresses simply superimpose on the present results. Quasistatic analysis is undertaken. In most of the subsequent analysis, the Poisson ratio, ν, was kept constant with z to simplify the discussions ($0 \leqslant \nu < 1/2$). In selected cases, a Poisson ratio variation of the type, $\nu = \nu_\infty - (\nu_\infty - \nu_0)e^{-z/l}$ was used, with ν_0 being the Poisson ratio at the surface ($z = 0$), ν_∞ the Poisson ratio far away from the free surface ($z \to \infty$), and $l \geqslant 0$ a characteristic length associated with the Poisson ratio decay. High values of Poisson ratio ($\nu \to 0.5$) correspond to situations of saturated soils (undrained condition) or to the commencement of plasticity. A comprehensive study of the influence of Poisson ratio was undertaken by systematically varying its average value.

Two classes of elastic inhomogeneity, pertinent to engineering materials and geomechanics, were examined. The inhomogeneity distributions were selected to represent

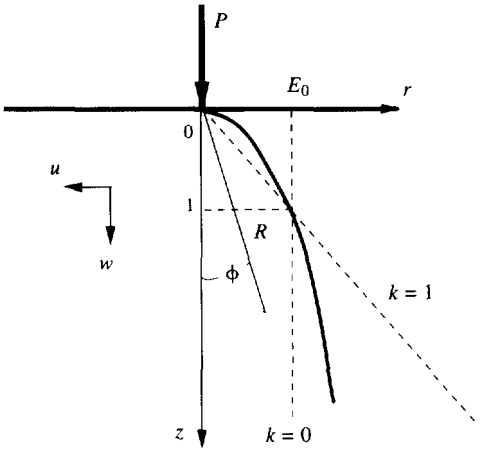

Fig. 1. The power law model, $E = E_0 z^k$ ($0 \leqslant k < 1$).

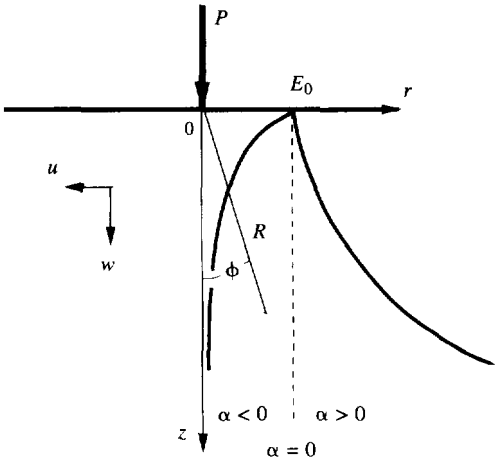

Fig. 2. The exponential law model, $E = E_0 e^{\alpha z}$ ($E_0 > 0$).

general morphologies of the elastic modulus encountered in such problems, as well as to be amenable to analytic or semi-analytic solutions.

- In the first group of model materials, the Young's modulus, E, depends on the depth, z (see Fig. 1) according to a simple power law, $E = E_0 z^k$. Note that E_0 has dimensions of stress $\times$ length^{-k}. For decaying values of stresses with depth, the power exponent must be constrained to be $0 \leqslant k < 1$. This model adequately describes many dense sand and clay earth deposits. At the surface the stiffness is very small; it, however, increases continuously with depth.
- In the second group of model materials, Young's modulus varies with z according to an exponential law, $E = E_0 e^{\alpha z}$. In this formulation, E_0 has ordinary dimensions of stress, whereas α has dimensions of length^{-1}. Therefore, this inhomogeneity description introduces a characteristic length to the problem, which is $1/\alpha$ when $\alpha \neq 0$ (see Fig. 2). A surface which is more compliant than the substrate is indicated by $\alpha > 0$, whereas a stiffer surface is indicated by $\alpha < 0$.

Let (r, z) be the axisymmetric polar coordinates for an elastic half space, $z \geqslant 0$, with corresponding displacements (u, w). The circumferential displacement vanishes and all the relevant functions are independent of the circumferential coordinate, θ. In the absence of body forces, there are only two stress equilibrium equations:

$$\frac{\partial \sigma_{rr}}{\partial r} + \frac{\partial \sigma_{rz}}{\partial z} + \frac{\sigma_{rr} - \sigma_{\theta\theta}}{r} = 0, \quad \frac{\partial \sigma_{rz}}{\partial r} + \frac{\partial \sigma_{zz}}{\partial z} + \frac{\sigma_{rz}}{r} = 0. \tag{1}$$

The strains are related to the displacements as

$$\varepsilon_{rr} = \frac{\partial u}{\partial r}, \quad \varepsilon_{zz} = \frac{\partial w}{\partial z}, \quad \varepsilon_{\theta\theta} = \frac{u}{r}, \quad \gamma_{rz} = \frac{\partial u}{\partial z} + \frac{\partial w}{\partial r} \tag{2}$$

and the volumetric strain is

$$\Theta = \frac{\partial u}{\partial r} + \frac{u}{r} + \frac{\partial w}{\partial z}. \tag{3}$$

Hook's law for an isotropic, compressible ($\nu \neq 1/2$), inhomogeneous material is written in terms of displacements as

$$\sigma_{rr} = 2\mu\left\{\frac{\partial u}{\partial r} + \frac{\nu}{1-2\nu}\Theta\right\}, \quad \sigma_{zz} = 2\mu\left\{\frac{\partial w}{\partial z} + \frac{\nu}{1-2\nu}\Theta\right\}, \tag{4a}$$

$$\sigma_{\theta\theta} = 2\mu\left\{\frac{u}{r} + \frac{\nu}{1-2\nu}\Theta\right\}, \quad \sigma_{rz} = \mu\left\{\frac{\partial u}{\partial z} + \frac{\partial w}{\partial r}\right\}, \tag{4b}$$

where $\mu = E/[2(1+\nu)]$ is the shear modulus which may generally depend on z.

Before closing this section, we point to the relevance of the choice of present model material systems to both geomechanics and structural materials. The values of shear modulus, typical of sandy soils and normally consolidated clay deposits, varies with depth beneath the earth surface as (O'Neill and Dobry, 1980) $\mu = 88440 K z^{0.5}$, where $K = 30$–150 Pa m$^{-1/2}$, z is in m and μ in Pa. For these cases, the Poisson ratio is $\nu = 0.4$. Various profiles of the elastic modulus from actual geomechanical tests resemble the present models (e.g., Judd, 1964; Kezdi and Lazanyi, 1976; Dowding, 1978; Pariseau, 1984; Prakash, 1984; Pells, 1985; Bell *et al.*, 1990). Examples of power law modulus variations can be found in the Gault clay at Cambridge, U.K., as well as sandy soils and normally consolidated clay deposits. Typical cases of linear (trapezoidal) elastic modulus distribution are London's clay, chalk and Pliocene clays. Exponentially decreasing elastic modulus usually occurs in glacial clays at Redcar, U.K., and the sensitive clay in Ottawa, Canada. Typical cases of

exponentially increasing elastic modulus are glacial clays at Cowden and Garston, U.K., chalk at Luton, U.K., and Pliocene fine-grained clays. For structural engineering materials comprising compositionally graded metal-ceramic layers, such as the Ni-aluminum oxide graded multilayers which have been the model systems of a number of recent research studies (e.g., Finot *et al.*, 1994; and Suresh and Needleman, 1996), the variation of Young's modulus with depth can be well approximated by $E = 84.9z^{0.216}$, with z in μm and E in GPa (with the free surface taken from the soft region, i.e., pure Ni). The Poisson ratio is assumed to be $v = 0.3$ everywhere in the composite. The same material, but with the free surface taken from the hard region (pure Al_2O_3) can be well approximated by $E = 380e^{-0.000332z}$, with z in μm and E in GPa.

3. ANALYTICAL RESULTS

3.1. *The power law case*: $E = E_0 z^k$

3.1.1. *The point force problem with radial fields.* As has been found earlier by Holl (1940), Hruban (1958) and Lekhniskii (1962), it is impossible, in general, to have a radial distribution of stresses in a point force problem. That is, the stresses cannot be aligned in the radial direction with an epicenter at the point of application of the concentrated force P. There is but only one radial solution which is related to the particular gradient of the elastic properties and connects k with the Poisson ratio v. It is useful to briefly examine here the basic results of this particular case, to set the scene for several key analytical formulations of the present work.

Consider spherical coordinates (R, ϕ, θ), see Fig. 1, and assume that the radial stress, σ_{RR}, is the only non-zero stress. From equilibrium and radial symmetry, $\partial\sigma_{RR}/\partial R + 2\sigma_{RR}/R = 0$,

$$\sigma_{RR} = R^{-2}S(\phi), \tag{5}$$

where $S(\phi)$ is a function of the spherical angle ϕ, as shown in Fig. 1. Note that the form of eqn (5) is prescribed *a priori* and it defines the essential radiality of the stresses. Moreover, σ_{RR}, is the only principal stress in this case, and eqn (5) satisfies automatically the stress-free boundary conditions at the surface ($\phi = \pi/2$), $\sigma_{\phi\phi} = \sigma_{R\phi} = 0$. The non-zero strains are:

$$\varepsilon_{RR} = \varepsilon, \quad \varepsilon_{\theta\theta} = \varepsilon_{\phi\phi} = -v\varepsilon. \tag{6a}$$

Compatibility (strain-displacement) equations are in this case

$$\varepsilon_{RR} = \frac{\partial u_R}{\partial R}, \quad \varepsilon_{\phi\phi} = \frac{u_R}{R} + \frac{1}{R}\frac{\partial u_R}{\partial \phi}, \quad \varepsilon_{\theta\theta} = \frac{u_R}{R} + \frac{u_\phi}{R}\cot\phi, \quad \gamma_{R\phi} = \frac{\partial u_\phi}{\partial R} - \frac{u_\phi}{R} + \frac{1}{R}\frac{\partial u_R}{\partial \phi}, \tag{6b}$$

where (u_R, u_ϕ) are the displacements along R and ϕ coordinates. Equations (6a) and (6b) give

$$\varepsilon_{RR} = AR^{-1/v}\cos\phi + BR^{-1-1/v}, \tag{7}$$

where A and B are constants.

For Hook's law to be valid, $E = \sigma_{RR}/\varepsilon_{RR}$, $B = 0$, $A = C/E_0$ and $k = (1/v) - 2$; thus the critical Poisson ratio, $v_{cr} = 1/(k+2)$. The problem is completed by stating the angular distribution of stress,

$$S(\phi) = C(\cos\phi)^{1/v-1} \tag{8}$$

where C is a constant, and the displacement fields are:

$$u_R = \frac{C}{E_0}\frac{v}{v-1}R^{1-1/v}\cos\phi, \quad u_\phi = -\frac{C}{E_0}\frac{v^2}{v-1}R^{1-1/v}\sin\phi. \tag{9}$$

Global equilibrium connects the constant C with the applied vertical load P at the surface origin as

$$2\pi C\int_0^{\pi/2}(\cos\phi)^{1/v+1}\,\mathrm{d}\phi = -P. \tag{10}$$

As an example, typical of many types of clay and sand, consider the case of $E = E_0\sqrt{z}$. Then for a Poisson ratio, $v = 0.4$, the non-zero components of the fields are

$$\sigma_{RR} = \frac{-7P}{4\pi R^2}\cos^{3/2}\phi, \quad u_R = \frac{7P}{6\pi E_0 R^{3/2}}\cos\phi, \quad u_\phi = \frac{-7P}{15\pi E_0 R^{3/2}}\sin\phi, \tag{11}$$

where $\phi = \pi/2$ at the surface and $\phi = 0$ along the z-axis.

The present section is closed by recalling the particular case of $k = 1$ (Gibson soil, $E = E_0 z$) and $v = 0.5$ (incompressibility). Gibson and Kalsi (1974) and Callandine and Greenwood (1978) proved that a simple radial field exists in this case and that it follows the distribution of the homogeneous case. In the spherical coordinate system (R, ϕ, θ), it was found that the non-zero components of displacements, strains and stresses, respectively, are

$$u_R = C/R^2, \quad \varepsilon_{RR} = -2C/R^3, \quad \varepsilon_{\theta\theta} = \varepsilon_{\phi\phi} = C/R^3, \quad \sigma_{RR} = \frac{-2CE_0\cos\phi}{R^2}, \tag{12}$$

with $C = 3P/(4\pi E_0)$. The displaced volume gives a remarkable relation between indentation displacement and contact stress, which are simply related with a Winkler type of spring constant of magnitude $2E_0/3$ (Callandine and Greenwood, 1978).

Although the previous results had been known (Holl, 1940; Hruban, 1958), the effect of the Poisson ratio for value above the critical value, $1/(k+2)$, has not been examined thus far. This effect will be explored in a later section with full field finite element calculations.

3.1.2. *The Flamant and Boussinesq problems for the power law case.* We develop in this section general solutions for line and point load problems for the power law case. As shown earlier, if the Poisson ratio v is not related to the power law exponent k according to $k = 1/v - 2 (0 \leqslant k < 1)$, then a simple radial field cannot be constructed for the axisymmetric Boussinesq problem (point force). However, since the elastic property distribution does not contain any characteristic length, it is possible to use potential theory to extract closed form results. We solve first the Flamant problem, i.e., the solution for a vertical line load (plane strain). The solution to the point load that corresponds to the axisymmetric Boussinesq problem can be derived from it by recourse to Aleksandrov's theorem which connects the axisymmetric and plane problems (Aleksandrov, 1961). The approach of Booker *et al.* (1985) was to integrate directly the equilibrium equations in spherical coordinates. The following method utilizes a different approach which involves the equilibrium equations in cylindrical coordinates and the connection between axisymmetric and plane problems. As shown later, the present results converge to the solution of Booker *et al.* in specific cases.

In the governing two dimensional compatibility equations, the stresses are expressed in terms of the Airy stress function (e.g., Ching-Hua, 1961). Expressing the compatibility equation in polar coordinates (R, ϕ)† and assuming a state of radial stress, and using

† The present approach with cylindrical coordinates, albeit more cumbersome than with the spherical coordinates for the power law case, is much more versatile because of its use for arbitrary variations of elastic moduli (especially for the cases that contain intrinsic lengths such as the exponential model discussed earlier).

axisymmetry, the stress solution can be written as

$$\sigma_{RR} = -CPR^{-1}(\sin\phi)^k \cos\left(q\frac{\pi-\phi}{2}\right). \tag{13}$$

From global equilibrium

$$C = \frac{1}{\pi\Gamma(2+k)} \times 2^{1+k}\Gamma\left(\frac{3+k+q}{2}\right)\Gamma\left(\frac{3+k-q}{2}\right), \tag{14}$$

where $\Gamma(\ )$ is the Gamma function (Magnus and Oberhettinger, 1954) and q is a function defined as $\sqrt{(1+k)[1-kv/(1-v)]}$. The normal strain in terms of the Airy function is

$$\varepsilon_{zz} = \frac{\partial w}{\partial z} = \frac{1}{\mu}\left(-\frac{\partial^2 F}{\partial z^2} + (1+v)\Delta F\right), \tag{15}$$

where $x = R\sin\phi$, $z = R\cos\phi$, $\Delta = \partial^2/\partial x^2 + \partial^2/\partial z^2$. Integrating ε_{zz} for the vertical displacement w at the surface, leads to

$$w(x, z=0) = \frac{(1-v^2)qCP}{E_0(1+k)k}|x|^{-k}\sin\frac{\pi q}{2}. \tag{16}$$

If $P = 1$, the above form serves as the kernel for the 2-D contact problems.

Returning to the Boussinesq problem, and using the Aleksandrov (1961) theorem, the surface displacement is written as

$$w(r, z=0) = \frac{-P}{\pi}\int_r^\infty \frac{\partial}{\partial x}(w(x, z=0))\frac{\mathrm{d}x}{\sqrt{x^2-r^2}}. \tag{17}$$

Rearranging the terms and using the integral properties of Gamma functions, the vertical surface displacement for a point force of a power law elastic modulus distribution is

$$w(r, z=0) = \frac{(1-v^2)}{2E_0}\frac{CqP\sin(\pi q/2)}{(1+k)r^{1+k}\sqrt{\pi}}\frac{\Gamma(1/2+k/2)}{\Gamma(1+k/2)}. \tag{18}$$

In a similar way, the radial surface displacement becomes

$$u(r, z=0) = \frac{(1-v^2)}{E_0}\frac{CP\cos(\pi q/2)}{kr^{1+k}\sqrt{\pi}}\frac{\Gamma(1+k/2)}{\Gamma(1/2+k/2)}, \tag{19}$$

with C defined in eqn (14).

The above results are the same as those of Booker *et al.* (1985) and Rostovtsev and Khranevskaia (1971), where the latter give additionally the stress σ_{zz} along the z-axis of the applied vertical load

$$\sigma_{zz}|_{r=0} = \frac{-3P}{2\pi}Mz^{-2}, \tag{20}$$

Table 1. Theoretical values of M for different ν and k values and M values derived from finite element simulations

ν	k	q^*	$M\dagger$	$M\ddagger$
1/3	1/8	1.026980	1.063809	1.06
1/3	1/2	1.060670	1.215811	1.19
1/3	7/8	1.026980	1.308136	1.24
1/4	1/8	1.037821	1.030632	1.04
1/4	1/2	1.118034	1.349478	1.37
1/4	7/8	1.153698	1.452385	1.49

* $q = \sqrt{\{(1+k)[1-k\nu/(1-\nu)]\}}$.
† Equation (21).
‡ Finite element results.

where

$$M = \frac{(k+3)(k+2)}{6}\left[\frac{1}{(5+k-q)(3+k-q)}F\left(2,k+4;\ \frac{7+k-q}{2};\ \frac{1}{2}\right)\right.$$
$$\left. + \frac{1}{(5+k+q)(3+k+q)}F\left(2,k+4;\ \frac{7+k+q}{2};\ \frac{1}{2}\right)\right] \quad (21)$$

and F is the Gauss hypergeometric function. The theoretically predicted values of M are compared in Table 1 with our computational results.

Along the surface ($z = 0$), all stresses are zero. It can be further shown that along the z-axis, σ_{rr} and $\sigma_{\theta\theta}$ are principal stresses and

$$\sigma_{rr}|_{r=0} = \sigma_{\theta\theta}|_{r=0}, \quad \sigma_{rz}|_{r=0} = 0, \quad (22a)$$

$$\sigma_{rr}|_{r=0} = -PC\left(z^k(1+\nu)\int_0^r \frac{x^2\cos(q\,\mathrm{atan}(x/z))}{(x^2+z^2)^{(k+3)/3}\sqrt{r^2-x^2}}\mathrm{d}x\right.$$
$$\left. + z^{k+2}\nu\int_0^r \frac{\cos(q\,\mathrm{atan}(x/z))}{(x^2+z^2)^{(k+3)/3}\sqrt{r^2-x^2}}\mathrm{d}x\right)\Bigg|_{r\to 0}. \quad (22b)$$

Denoting by (R, ϕ) the polar coordinates in the (r, z) plane, the stresses can be generally expressed as

$$\sigma_{ij} = R^{-2}S_{ij}(\phi), \quad (23)$$

where S_{ij} $(i,j = R, \phi, \theta)$ depend on k and ν and can be given analytically in the most general case only for $\nu = 1/(k+2)$ (see previous section). Booker *et al.* (1985) solved numerically the case of $\nu = 0.25$ and $0 \leqslant k \leqslant 1$.

Some general analytic results can be further deduced from the equilibrium equation along the z-axis:

$$\partial\sigma_{\theta\theta}/\partial\phi = 0, \quad \partial\sigma_{zz}/\partial\phi = 0, \quad \partial\sigma_{rr}/\partial\phi = 0, \quad \partial\sigma_{rz}/\partial\phi = -\sigma_{zz}. \quad (24)$$

The separation of variables in the form of eqn (23), implies that $\sigma_{\theta\theta} = 0$ is a straight line starting from the origin. $\sigma_{\theta\theta}$ is a principal stress, and using the 3-D Mohr's circles, it can be shown that the location of the line of $\sigma_{\theta\theta} = 0$ coincides with the line of maximum shear stress σ_{rz}.

Clearly, the stresses do not depend on E_0, are proportional to the applied load, P, and decay to zero as z^{-2} with depth ($z \to \infty$), as expected. The previous results converge to the classic Boussinesq (1885) solution for the homogeneous case when $k = 0$ (Appendix 1 gives a short summary for comparison).

3.2. *The case of exponential variation in modulus*: $E = E_0 e^{\alpha z}$

3.2.1. *The general axisymmetric problem for the exponential law case.* In this section we develop solutions for the constant pressure and the point load problem assuming the exponential variation of modulus. We begin by examining the equilibrium eqns (1). Assuming sufficient continuity for the displacements, borrowing from the homogeneous analysis of axisymmetric problems (Love 1927), we take an auxiliary function, $\kappa(r, z)$, related to the radial displacement u as

$$u = \frac{\partial \kappa}{\partial r}. \tag{25}$$

Inserting eqn (25) into the equilibrium eqns (1), and after eliminating the vertical displacement w, a partial differential equation is obtained with regard to the auxiliary function κ,

$$\Delta\Delta\kappa - a\Delta\kappa + 2\alpha \frac{\partial}{\partial z}\Delta\kappa + b\frac{\partial^2 \kappa}{\partial z^2} = 0, \tag{26}$$

where Δ is the Laplace operator for the axisymmetric problems and

$$a = \frac{\alpha^2 \nu}{1-\nu}, \quad b = \frac{\alpha^2}{1-\nu}. \tag{27}$$

Note that for the homogeneous case, $\alpha = 0$, we have $a = 0$ and $b = 0$, and the above equation reduces to Love's biharmonic function (Love, 1927). For the case of $\alpha \neq 0$, separation of the r and z variables in the form of Laplace transform, gives a set of two Bessel ordinary differential equations which give the solution in terms of the Bessel functions of zeroth, J_0, and first order, J_1. The appearance of the radial dimension in terms of Bessel functions was expected on the basis of the axisymmetric formulation of the problem. Keeping the arguments real, a solution for the auxiliary function that is relevant to the semi-infinite body ($z \leqslant 0$) reads as

$$\kappa(r, z) = \int_0^\infty e^{tz}[F_1(t)\cos(pz) + F_2(t)\sin(pz)]J_0(qr)\,dt, \tag{28}$$

where $F_1(t)$ and $F_2(t)$ are arbitrary functions to be determined from the boundary conditions at $z = 0$. The parameters q, p are related to the transformation parameter t as

$$q = (2t+\alpha)\sqrt{\frac{t(t+\alpha)}{a+(2t+\alpha)^2}}, \quad p = \sqrt{\frac{at(t+\alpha)}{a+(2t+\alpha)^2}} \tag{29}$$

and taking $t\alpha > 0$ ($t > 0$, if $\alpha > 0$; $t < 0$, if $\alpha < 0$).

The displacements take the form ($z \leqslant 0$)

$$u(r, z) = -\int_0^\infty e^{tz} q[F_1(t)\cos(pz) + F_2(t)\sin(pz)]J_1(qr)\,dt, \tag{30}$$

$$w(r, z) = \int_0^\infty e^{tz}(\Psi_1(r, t)\cos(pz) + \Psi_2(t)\sin(pz))J_0(qr)\,dt, \tag{31}$$

where

$$\Psi_1(r,t) = \frac{1}{p^2+\omega^2}[\omega\Phi_1(r,t)+p\Phi_2(r,t)], \tag{32a}$$

$$\Psi_2(r,t) = \frac{1}{p^2+\omega^2}[\omega\Phi_2(r,t)+p\Phi_1(r,t)], \tag{32b}$$

$$\Phi_1(r,t) = [q^2F_1(t)-(1-2v)\sqrt{a}qF_2(t)]J_0(qr), \tag{33a}$$

$$\Phi_2(r,t) = [q^2F_2(t)+(1-2v)\sqrt{a}qF_1(t)]J_0(qr) \tag{33b}$$

and

$$\omega = t+\alpha(1-2v). \tag{34}$$

Using the expressions for the displacements, the stresses can be expressed in an integral form. The results are not presented here because of space restrictions.

The functions $F_1(t)$ and $F_2(t)$ are determined from the boundary conditions at the surface ($z = 0$). Concentrating on the boundary conditions, let the contact pressure be denoted by

$$\sigma_{zz}|_{z=0} = -g(r/R), \tag{35}$$

for $0 \leqslant r \leqslant R$ (R is the contact radius), $\sigma_{zz} = 0$ outside the contact circle and $g(r/R) \geqslant 0$. In absence of shear surface tractions,

$$\sigma_{rz}|_{z=0} = 0, \tag{36}$$

for $0 \leqslant r < \infty$. For $v \neq 0$, a general solution can be found by noting that the shear traction at the surface becomes zero when

$$F_2(t) = -P(t)F_1(t), \tag{37}$$

with

$$P(t) = \frac{q^2\omega+qp\sqrt{a}(1-2v)+t(p^2+\omega^2)}{q^2p-q\omega\sqrt{a}(1-2v)+p(p^2+\omega^2)}. \tag{38}$$

Recalling the Fourier-Bessel integral properties (in essence inverting Hankel transforms of order zero), F_1 is recovered from the normal stress at the surface:

$$F_1(t) = -\frac{(1-2v)}{2\mu}\frac{1}{q}s(qR)\frac{Q(t)}{S(t)-P(t)T(t)}, \tag{39}$$

where

$$s(qR) = \int_0^{qR}(qs)g(s/R)J_0(qs)\,\mathrm{d}(qs), \tag{40}$$

$$Q(t) = 2\sqrt{\frac{t(t+\alpha)}{a+(2t+\alpha)^2}}+\frac{(2t+\alpha)^2(a+\alpha^2)}{2\sqrt{[a+(2t+\alpha)^2]^3[t(t+\alpha)]}}, \tag{41}$$

$$S(t) = \frac{1}{p^2+\omega^2}[-vq^2(p^2+\omega^2)+(1-v)(1-2v)tpq\sqrt{a} + (1-v)tq^2\omega+(1-v)q^2p^2+(1-v)(1-2v)pq\sqrt{a\omega}], \quad (42)$$

$$T(t) = \frac{1}{p^2+\omega^2}[2q^2pt(1-v)-qt\sqrt{a\omega}(1-v)(1-2v) + (1-v)(1-2v)q^2p\alpha-(1-v)(1-2v)qp^2\sqrt{a}]. \quad (43)$$

For a unit load, $g = 1$, $s(qR) = qRJ_1(qR)$ and the solution becomes

$$F_1(t) = -\frac{(1-2v)}{2\mu}RJ_1(qR)\frac{Q(t)}{S(t)-P(t)T(t)}. \quad (44)$$

3.2.2. *The special case of* $v = 0$ *for the exponential law case.* For the particular case of $v = 0$, a simpler analytic solution can be derived which can be very illuminating for subsequent discussions on the influence of material length in graded materials. In this case the parameters of the previous section simplify as

$$a = 0, \quad p = 0, \quad q = \sqrt{t(t+\alpha)}, \quad \omega = t+\alpha. \quad (45)$$

The displacements and stresses reduce to ($z \leqslant 0$)

$$u(r,z) = -\int_0^\infty e^{tz}qF_1(t)J_1(qr)\,dt, \quad w(r,z) = \int_0^\infty e^{tz}tF_1(t)J_0(qr)\,dt, \quad (46)$$

$$\sigma_{zz}(r,z) = E_0e^{|\alpha|z}\int_0^\infty e^{tz}J_0(qr)t^2F_1(t)\,dt, \quad \sigma_{rr}(r,z) = -E_0e^{|\alpha|z}\int_0^\infty e^{tz}q^2\frac{dJ_1(qr)}{d(qr)}F_1(t)\,dt, \quad (47)$$

$$\sigma_{\theta\theta}(r,z) = -E_0e^{|\alpha|z}\frac{1}{r}\int_0^\infty e^{tz}J_1(qr)qF_1(t)\,dt, \quad \sigma_{rz}(r,z) = -2E_0e^{|\alpha|z}\int_0^\infty e^{tz}qJ_1(qr)tF_1(t)\,dt. \quad (48)$$

The point force, P, applied at the surface origin ($r = 0, z = 0$) and directed in the z-axis (normal to the surface) can be solved exactly. The solution can be constructed using a limiting procedure from the uniform surface load to the concentrated load P. Changing the coordinate of the integration, the Boussinesq's problem for a point force, P, can be stated as

$$w(r) = \frac{P}{\pi E_0}\int_0^\infty G(q/\alpha)J_0(rq)\,dq \quad (49)$$

for the surface displacement, where

$$G(q/\alpha) = \frac{(2q/\alpha)\sqrt{(2q/\alpha)^2+1}}{(1+\sqrt{(2q/\alpha)^2+1})^2}. \quad (50)$$

The vertical stress, σ_{zz}, the radial, σ_{rr}, and the hoop stress, $\sigma_{\theta\theta}$, along the z-axis ($r = 0$) are principal stresses. It can be easily shown that

$$\sigma_{zz}|_{r=0} = \frac{P}{2\pi} e^{|\alpha|z} \int_0^\infty e^{tz} qQ \, dt, \quad \sigma_{rr}|_{r=0} = \frac{P}{4\pi} e^{|\alpha|z} \int_0^\infty e^{tz} \frac{q^2}{t^2} Q \, dt, \tag{51}$$

$$\sigma_{\theta\theta}|_{r=0} = \sigma_{rr}|_{r=0}, \quad \sigma_{r\theta}|_{r=0} = 0. \tag{52}$$

Some general analytic results can be further deduced from the equilibrium equation along the z-axis:

$$\partial\sigma_{\theta\theta}/\partial\phi = 0, \quad \partial\sigma_{zz}/\partial\phi = 0, \quad \partial\sigma_{rr}/\partial\phi = 0. \tag{53}$$

Note that $\sigma_{\theta\theta}$ is a principal stress and that using the 3-D Mohr's circles, the location of the line of $\sigma_{\theta\theta} = 0$ can be shown to coincide with the line of maximum shear stress σ_{rz}. For $\alpha < 0$, the stresses are proportional to the applied force, P, decay exponentially to zero for $z \to -\infty$, and do not depend on E_0, as expected. Along the z-axis, the vertical stress is the only compressive one, with the circumferential and radial stresses being tensile, as is the case for the homogeneous case. The coordinates scale with the absolute value of the characteristic length $1/|\alpha|$. Therefore, the Poisson ratio, v, completely determines the stress field for a unit load, $P = 1$. The situation is more complicated for $\alpha > 0$ and it appears that the stresses vary as z^{-2} with depth, a situation comparable to the power law case.

In the most general case, the influence function, G, is given in Appendix 2. In the homogeneous limit, $\alpha \to 0$, the results reduce exactly to the Boussinesq solution given in Appendix 1.

4. FINITE ELEMENT ANALYSIS

4.1. *Numerical formulation*

An axisymmetric mesh was constructed, as shown in Fig. 3. Four-noded, axisymmetric elements were used, with progressively varying element size. The final mesh had 4747 elements and 5058 nodes. Full integration scheme was used. No special types of elements were used, either close to the point force (so-called "singular elements") or at infinity (so-called "infinite elements"). The reason was that the solutions were sought with the simplest numerical scheme and for uniform treatment of the subsequent analysis of the various indenters (punch, cone and sphere). It is thus recognized that at distances very close and very far from the point force the solution is not accurate and only in-between the point of application of the force and the outer boundary is sufficient accuracy expected. The mesh was gradually refined to yield results in stresses that converged within less than 5% error when compared with all available analytic results, at distances more than three elements around the point of application of the force, P (see Table 1). The element size close to the origin (force point) was 1/840 to 1/1680 of the outer boundary total dimensions. The outer boundary was modeled with stress free conditions on the right side (side CD) and vertically constrained at the lower side (side AB in Fig. 3). In this way, it was possible to obtain a fine resolution of the fields, while simultaneously minimizing the modeling errors (since the far field boundary conditions were unknown, the specific finite element formulation can introduce boundary conditions which will influence the solution, if the mesh is small and inadequately designed with respect to the element distribution).

A numerical subroutine pertinent for the description of the inhomogeneity in the elastic and plastic properties at the element level was adopted (for isotropic and orthotropic mechanical response) (Giannakopoulos *et al.*, 1995), compatible with the ABAQUS (1993) general purpose finite element program. To the best of our knowledge, it is the first time that such code is developed and used in indentation problems with material properties that vary continuously with spatial coordinates. In addition, the code can handle any distribution of material properties, a fact that makes it extremely versatile. Allowing the material properties to vary within the individual elements provides enormous flexibility in meshing.

In all cases, a compressive force of magnitude $P = 1$ N was applied at the coordinate origin ($z = 0, r = 0$), which corresponds to a high distribution of pressure within the first

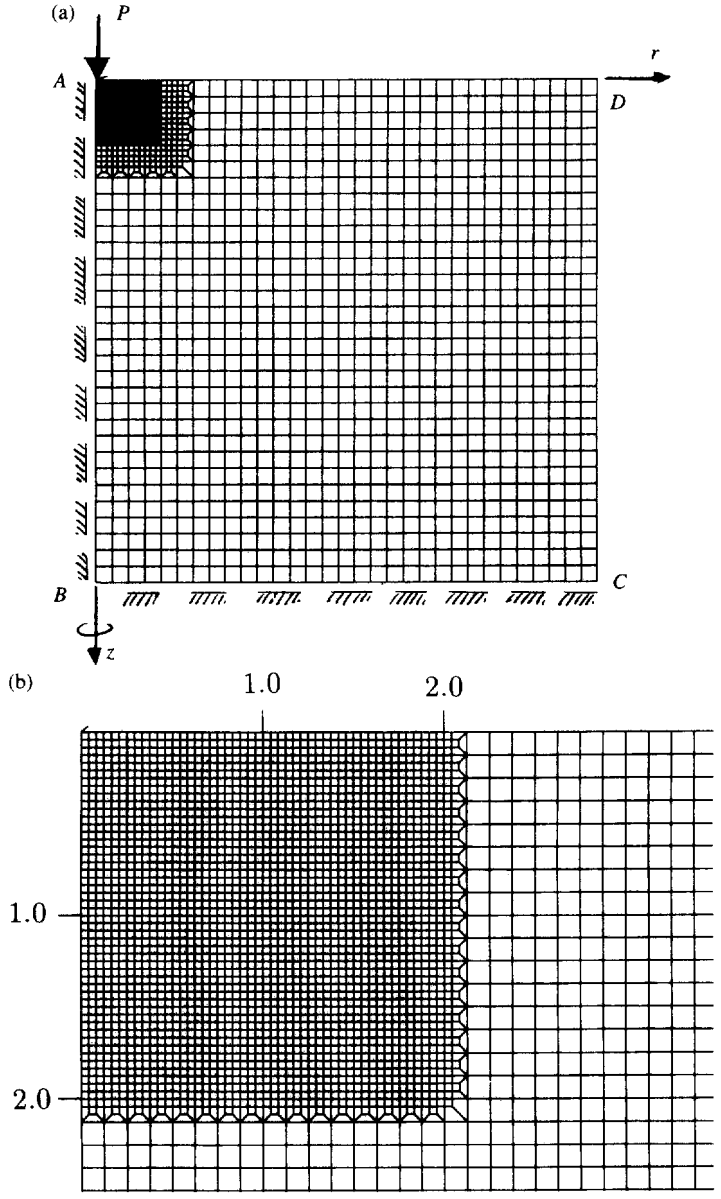

Fig. 3. (a) The overall view of the mesh used in the present calculations. (b) Details of the mesh close to the point force.

element at the origin. In line with the analysis, all results scale proportionally to the load P, a fact that was additionally verified numerically. From the analysis, it is clear that E_0 serves as a simple amplification factor for the strains and displacements, but does not affect either the distribution or the magnitude of the stress fields. The present computations confirm this, and a conventional value of $E_0 = 10^{11}$ Pa m^{-k} was used in the presented results. All lengths are in m and stresses in Pa. The problem is completely characterized by a fourth order stress vector whose components are presented in the form of two principal stresses (σ_1, σ_2) in the (r, z) plane, the circumferential stress, $\sigma_{\theta\theta}$ (which is also a principal stress) and the shear stress, σ_{rz} in the (r, z) plane. With this representation it is easy to transform the stresses to any other system, as well as to compute various types of effective stresses, such as the Mises and Tresca stresses and the pressure. Some general trends and comparisons of the results will be shown in Tables 2 and 3.

The successful solution of the present problems sets the stage for the solution of the actual indentation problems (punch, cone, sphere) to be presented in sequels to this paper (Giannakopoulos and Suresh, 1997). The present solutions may serve as far-field loads for elastic and elastoplastic analysis of indentation problems, since those solutions must

Table 2. A comparison of the indentation response of a homogeneous elastic medium and that of an elastic solid whose Young's modulus has a power law variation with depth beneath the indented surface

	Homogeneous (E_0)		Power law ($E_0 z^k$; $0 \leqslant k < 1$)		
	$\nu < 1/2$	$\nu = 1/2$	$\nu < \nu_{cr} = 1/(k+2)$	$\nu = \nu_{cr} = 1/(k+2)$	$\nu > \nu_{cr} = 1/(k+2)$
Surface deformation [$w(r)$]	More sinking-in than power law	Less sinking-in than $\nu < 1/2$	Less sinking-in than the homogeneous case		More sinking-in than $\nu < 1/(k+2)$
Dominant principal stress (σ_1)	Non-radial	Radial ($\sigma_1 = \sigma_{rr}$)	Non-radial, smaller than $\nu > 1/(k+2)$	Radial ($\sigma_1 = \sigma_{rr}$)	Non-radial, larger than $\nu < 1/(k+2)$
Secondary principal stress (σ_2)	Tensile	Zero	Tensile	Zero	Compressive
Circumferential stress ($\sigma_{\theta\theta}$)	Tensile along z-axis, compressive along surface	Zero	Tensile along z-axis, compressive along surface	Zero	Compressive along z-axis, tensile surface
Shear stress (σ_{rz})	Rotates towards z-axis	Rotates towards free surface	Rotates towards z-axis		Rotates towards free surface

Table 3. A comparison of the indentation response of a homogeneous elastic medium and that of an elastic solid whose Young's modulus has an exponential law variation with depth beneath the indented surface

	Homogeneous (E_0)	Exponential ($Ee^{\alpha z}$)		
	$\alpha = 0$ $0 \leqslant \nu < 1/2$	$\alpha < 0$ $0 \leqslant \nu < 1/2$	$\alpha > 0$ $\nu = 0$	$\alpha > 0$ $\nu = 0.4$
Surface deformation [$w(r)$]		More sinking-in than the homogeneous case	Less sinking-in than the homogeneous case	Less sinking-in than $\nu = 0$
Dominant principal stress (σ_1)	Focuses in the interior	Spreads more on the surface	Focuses in the interior, shows a clear steepest decent path	Similar to $\alpha = 0$
Secondary principal stress (σ_2)	Tensile, shows a clear steepest descent	Tensile, higher values than $\alpha = 0$	Tensile, lower values than for $\alpha < 0$, similar shapes to $\alpha = 0$	Mainly compressive, local maximum compression below the surface
Circumferential stress ($\sigma_{\theta\theta}$)	Tensile along z-axis, compressive along surface, zero values on a straight line from the origin	Tensile along z-axis, compressive along surface, zero values on an exponential curve from the origin that approaches depth $1/\lvert\alpha\rvert$	Higher values than $\alpha = 0$, but lower than $\alpha < 0$	Alternating tensile and compressive regions
Shear stress (σ_{rz})	Maximum values follow the $\sigma_{\theta\theta} = 0$ line	Maximum values follow the $\sigma_{\theta\theta} = 0$ curve	Maximum values directed more toward the interion than $\alpha = 0$	Similar to $\alpha = 0$

approach the present ones at distances sufficiently away from the indentation region where elastic conditions prevail. In this sense, the present results are analogous to the elastic crack-tip stress fields used extensively in linear and non-linear fracture mechanics. They can also be used for the creation of "singular" (near the point of the force application), as well as "infinite" (at the outer boundary), types of finite elements.

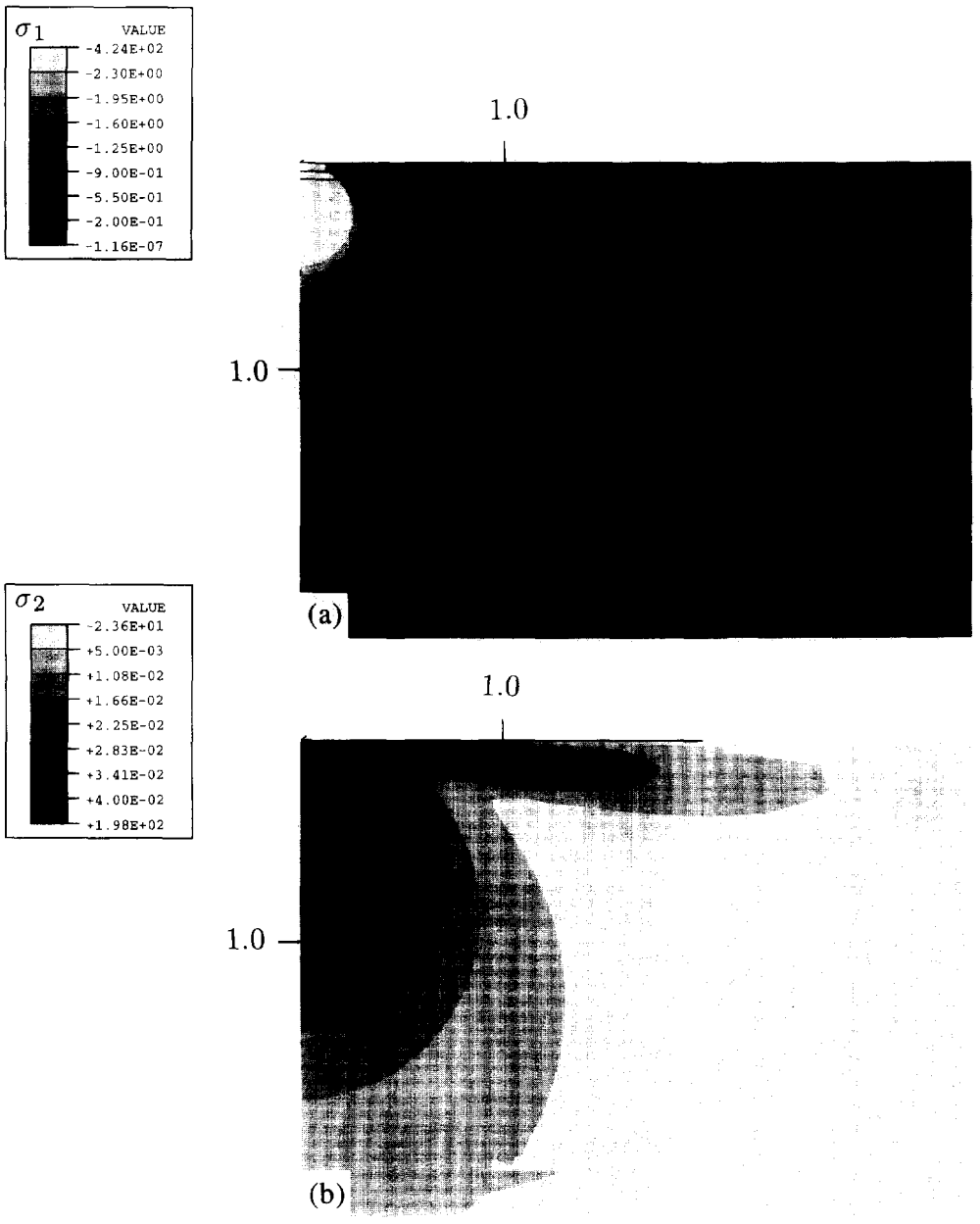

Fig. 4. The stress fields for $E = E_0 z^k$ with $k = 0.5$ and $\nu = 0.2$. (a) σ_1, the dominant principal stress, (b) σ_2, the secondary principal stress, (c) $\sigma_{\theta\theta}$, the circumferential stress, and (d) σ_{rz}, the shear stress (lengths are in m and stresses in Pa). (*Continued overleaf.*)

4.2. *The power law case*: $E = E_0 z^k$

For convenience in describing the stresses around the point force, we introduce the in-plane polar coordinates, R, ϕ, as indicated in Fig. 1 ($R^2 = r^2 + z^2$, $\tan\phi = r/z$). The ϕ-variation of the stresses and displacements derived for $\nu = 0.25$ and various values of k, as computed by Booker *et al.* (1985), were verified.† The stress singularity is R^{-2}, the strain singularity is $R^{-(2+k)}$ and the displacement singularity is $R^{-(1+k)}$. This gives a very good assessment of our finite element method for the power law material model and sets a good degree of confidence for the cases that follow.

† Booker *et al.* (1985), however, by using a Poisson ratio of 0.25 which is always less than the critical value of $1/(k+2)$ for $0 \leqslant k \leqslant 1$, did not capture some subtle issues of the stress distributions pertaining to the transition of the Poisson ratio from $\nu < 1/(k+2)$ to $\nu > 1/(k+2)$. In the present analysis, it was found that the Poisson ratio has an important influence on the stress distributions; it acts as an internal constraint in relation to the elastic modulus distribution characterized by the power exponent k.

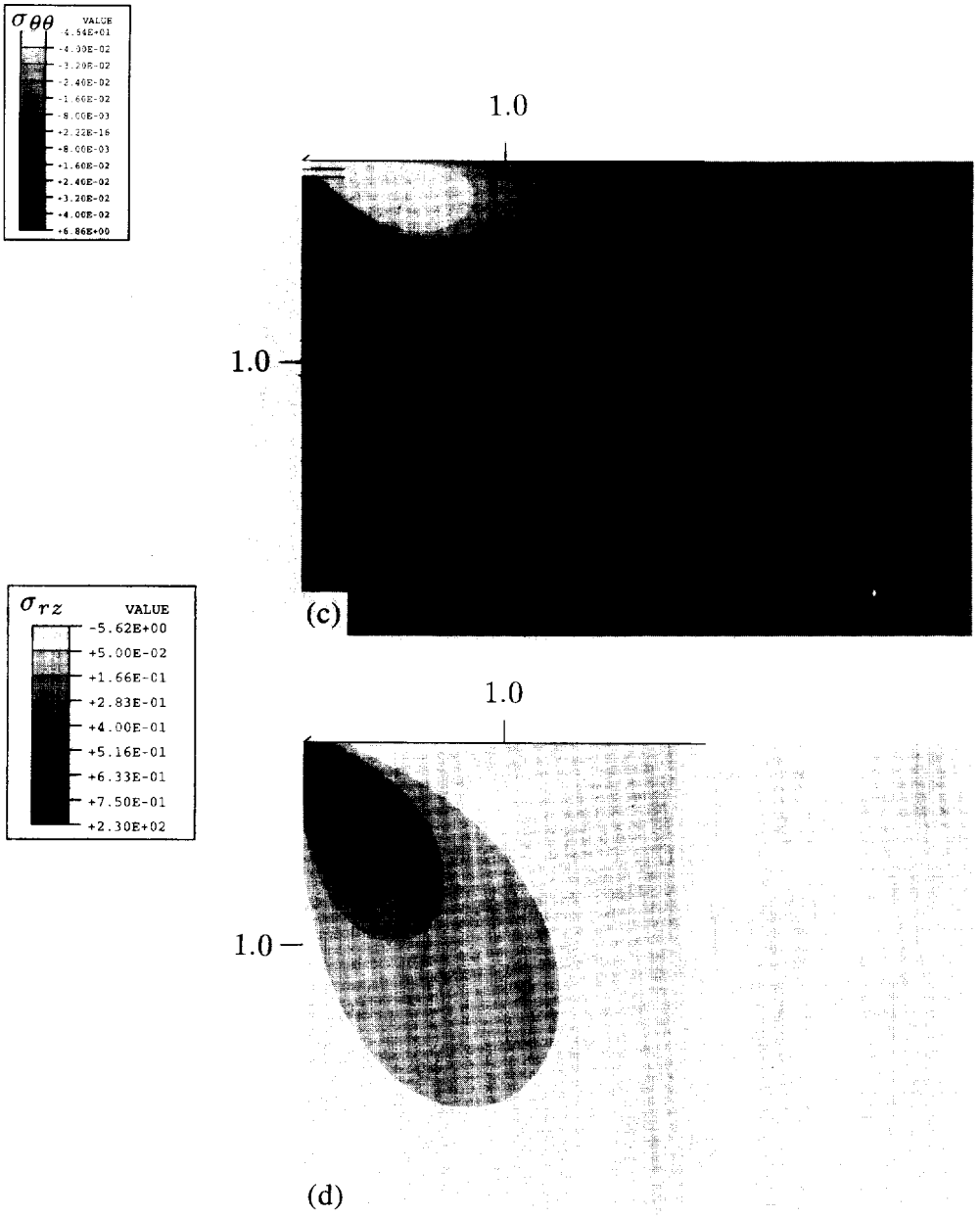

Fig. 4—*Continued.*

Analyses were done for $k = 0.00, 0.25, 0.50, 0.75, 1.00$, and for each k value the Poisson ratio was taken $\nu = 0.2$, $1/(k+2)$, 0.43, 0.45 (that is below, at and above its critical value). For $\nu = 1/(k+2)$, the fields are uniquely presented by the only non-zero principal stress, σ_1, and the shear stress, σ_{rz}. Regarding all the other cases, four stresses $(\sigma_1, \sigma_2, \sigma_{\theta\theta}, \sigma_{rz})$ are shown in sequence for complete description of the fields, as explained previously. For brevity, only the cases of $k = 0.50$ and 0.75 are shown, see Figs 4–9. Once ν and k are given, the results are universal and scale proportionally to the applied force, P.

As general trends, all stresses become zero at the surface, $z = 0$, as expected from the constitutive assumption $(E(z = 0) = 0)$. The shear stress, σ_{rz}, also becomes zero along the z-axis, as expected from the axisymmetric deformation. The principal stresses, σ_1, σ_2, are identical to σ_{zz} and σ_{rr}, respectively, along the z-axis. As expected from the theory, $\sigma_2 = \sigma_{\theta\theta}$ along the z-axis. In all cases, σ_1 is compressive (negative). We will term σ_1 as the dominant principal stress and σ_2 as the secondary principal stress, since in absolute magnitudes $|\sigma_1| \approx 6/(1-2\nu)|\sigma_2|$. The absolute value of the dominant principal stress, $|\sigma_1|$, increases by about 33% as k increases from $k = 0$ to 1, and decreases with increasing ν. The absolute

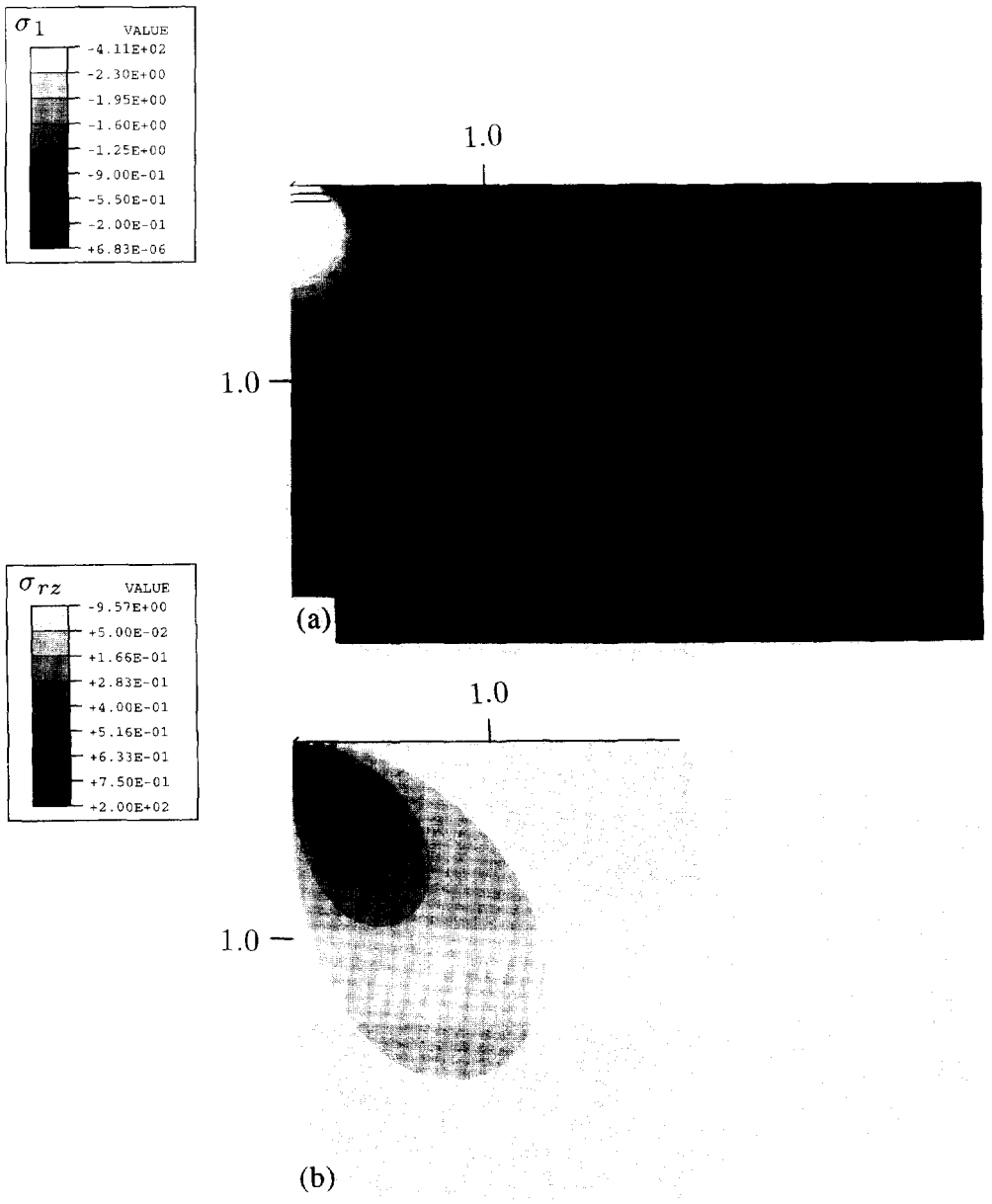

Fig. 5. The stress fields for $E = E_0 z^k$ with $k = 0.5$ and $\nu = 0.4$. (a) σ_1, and (b) σ_{rz}, shear stress (lengths are in m and stresses in Pa).

value of the secondary principal stress $|\sigma_2|$ decreases with k by about 4-fold as k increases from $k = 0$ to $k = 1$.

Perhaps the most dramatic effect is the change of sign of σ_2 and $\sigma_{\theta\theta}$ as the Poisson ratio ν increases past the critical value $1/(k+2)$. Table 2 summarizes the key trends corresponding to this variation, and compares the indentation response of the graded elastic medium with that of a medium with homogeneous elastic properties.

For $\nu < 1/(k+2)$, $\sigma_{\theta\theta}$ changes sign from positive values along the z-axis to negative values close to the free surface. The maximum positive value of the circumferential stress, $\sigma_{\theta\theta}$, appears along the z-axis and the maximum negative values appear at $\phi \approx 65^\circ$ for $k = 0$, increasing to $\phi \approx 85^\circ$ for $k = 0$. For $\nu > 1/(k+2)$, $\sigma_{\theta\theta}$ changes sign from negative values along the z-axis to positive values close to the free surface and becomes zero along a line $\phi \approx 45^\circ$ (decreases from around $\phi \approx 52.5^\circ$ at $k = 0$, to $\phi \approx 39^\circ$ at $k = 1$). The maximum negative value of $\sigma_{\theta\theta}$ appears along the z-axis and the maximum positive values appear at $\phi \approx 65^\circ$ for $k = 0$, increasing to $\phi \approx 85^\circ$ for $k = 1$. This effect is very important in the context of damage evolution in brittle materials and it indicates that damage may relocate

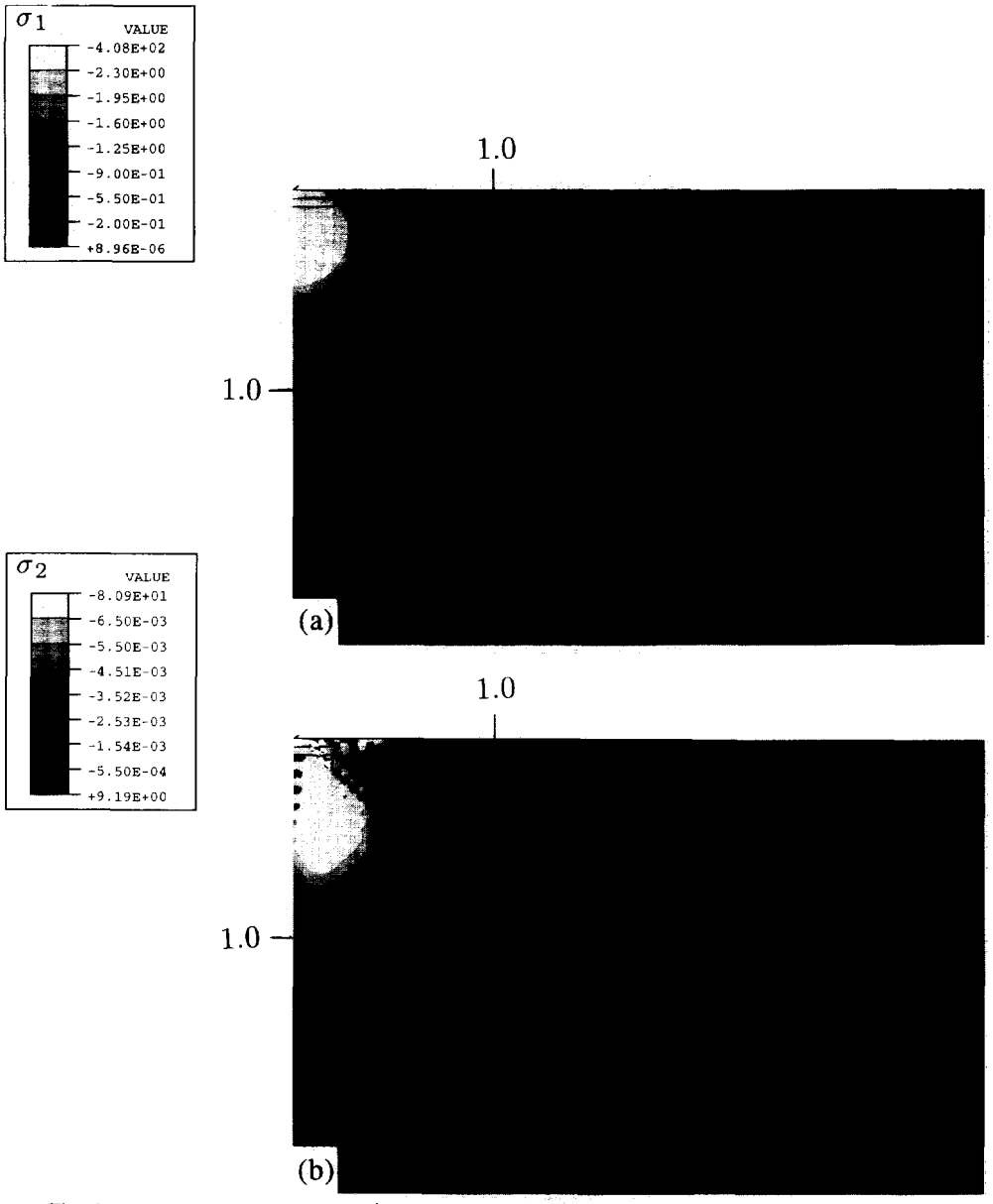

Fig. 6. The stress fields for $E = E_0 z^k$ with $k = 0.5$ and $\nu = 0.43$. (a) σ_1, (b) σ_2 and (c) $\sigma_{\theta\theta}$, (d) σ_{rz} (lengths are in m and stresses in Pa). (*Continued opposite.*)

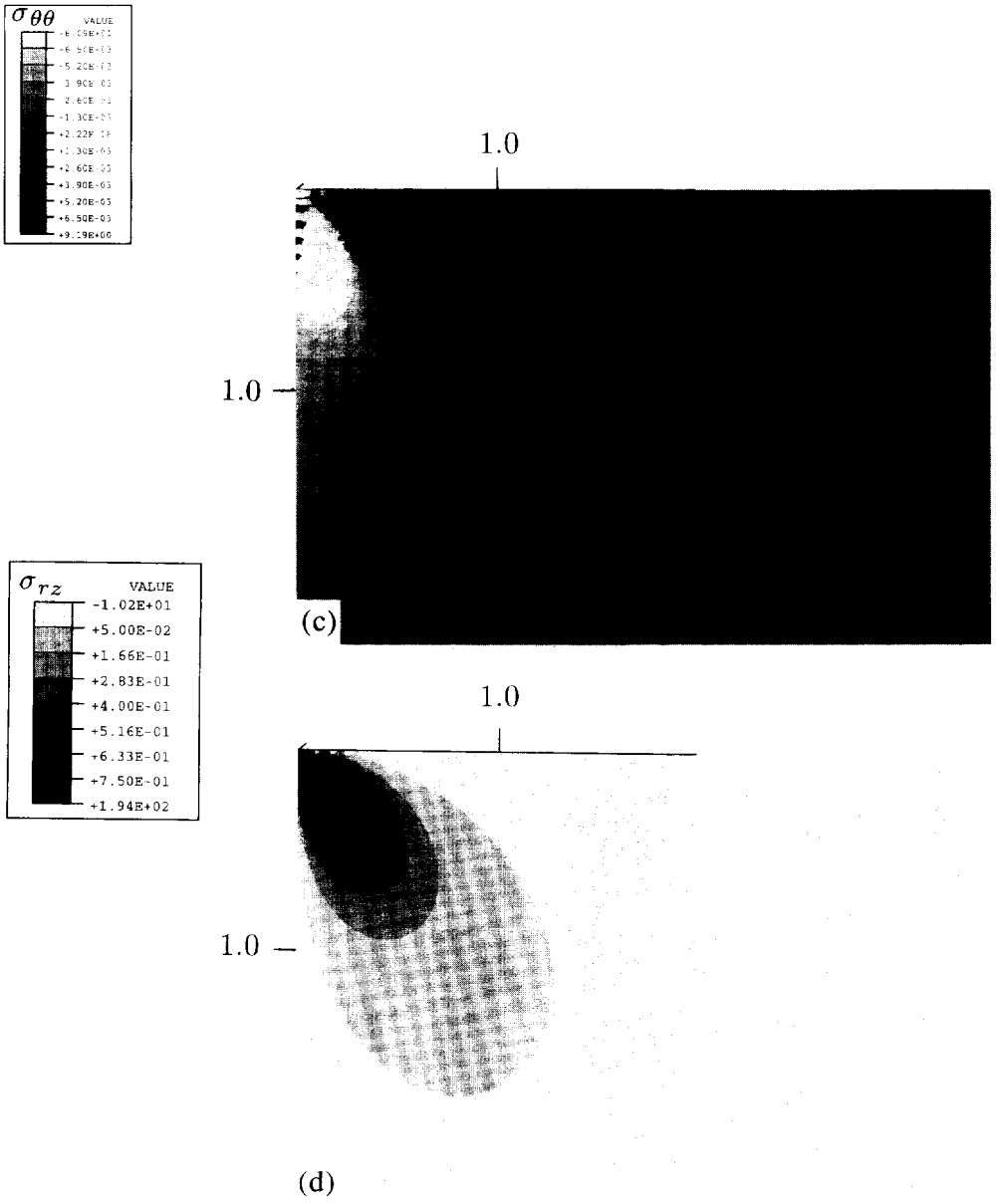

Fig. 6—*Continued.*

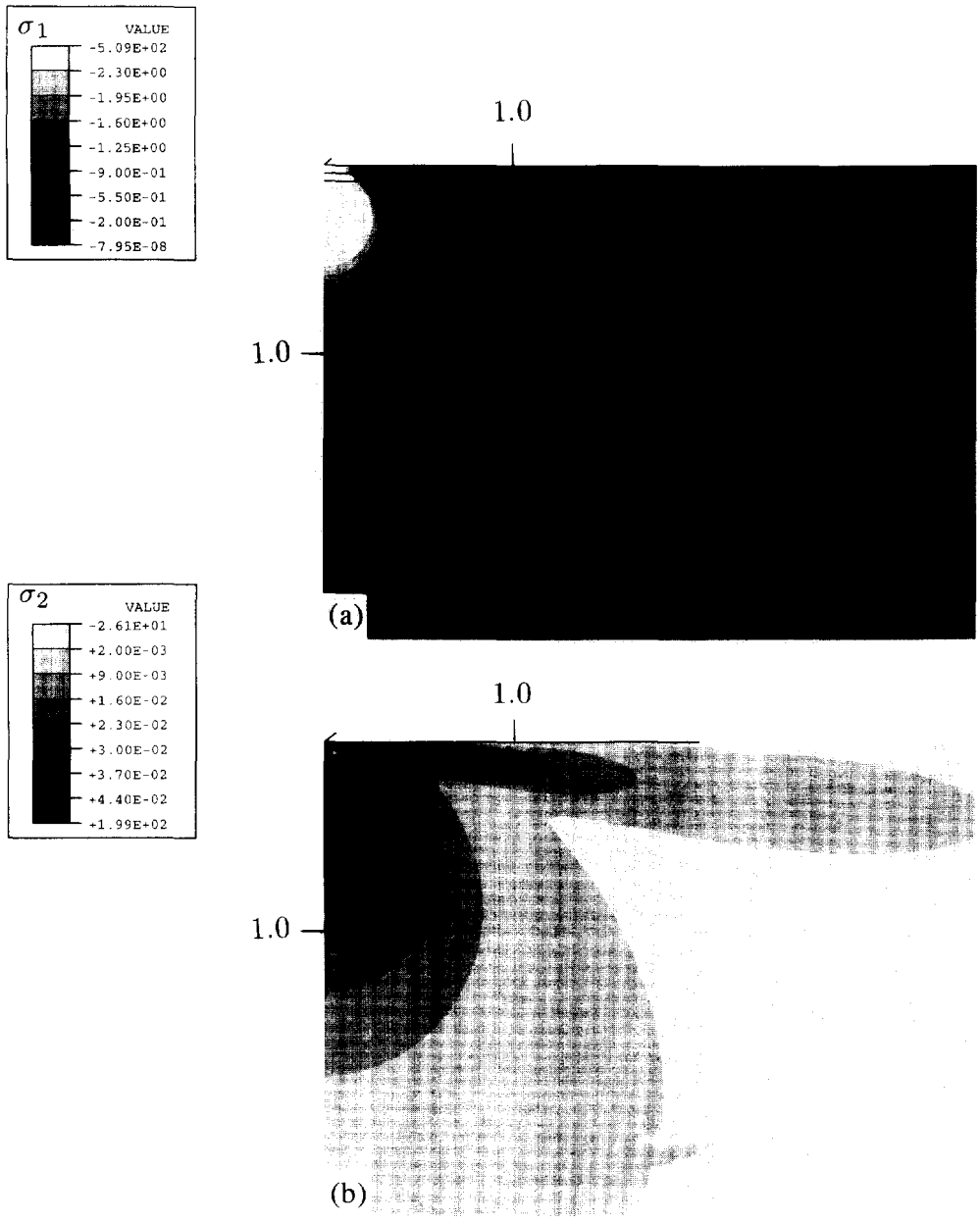

Fig. 7. The stress fields for $E = E_0 z^k$ with $k = 0.75$ and $\nu = 0.2$. (a) σ_1, (b) σ_2, (c) $\sigma_{\theta\theta}$, (d) σ_{rz} (lengths are in m and stresses in Pa). (*Continued opposite.*)

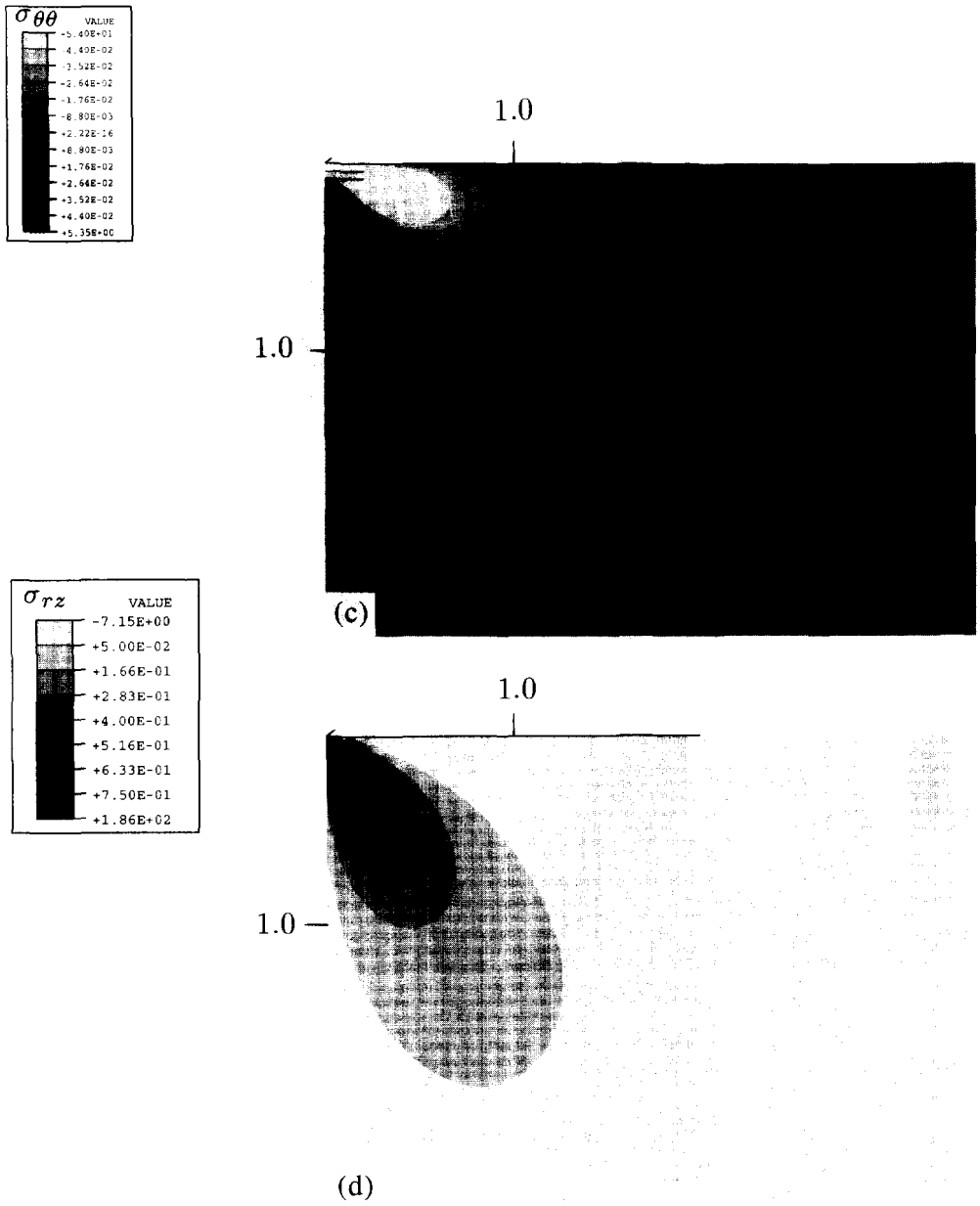

Fig. 7—*Continued.*

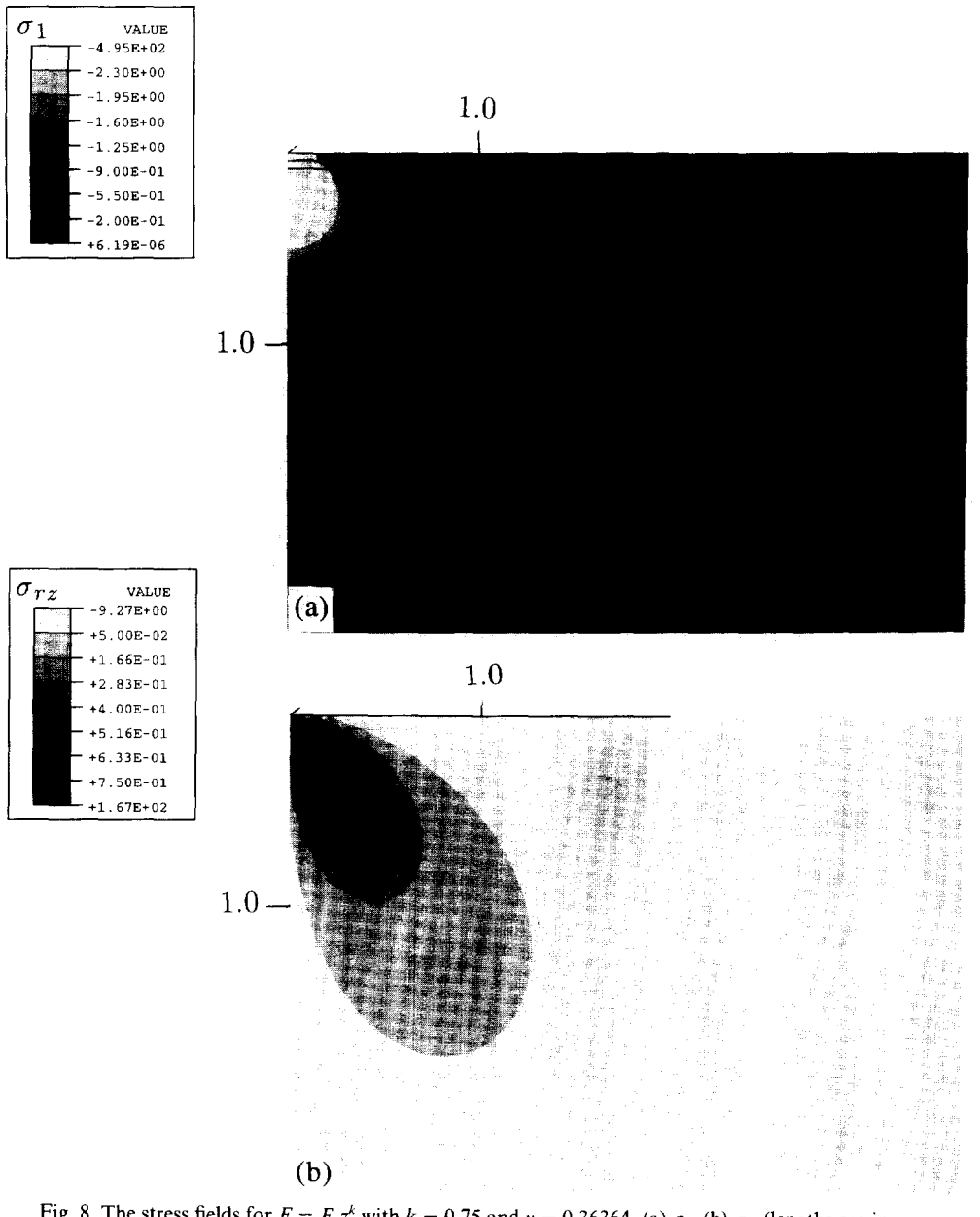

Fig. 8. The stress fields for $E = E_0 z^k$ with $k = 0.75$ and $\nu = 0.36364$. (a) σ_1, (b) σ_{rz} (lengths are in m and stresses in Pa).

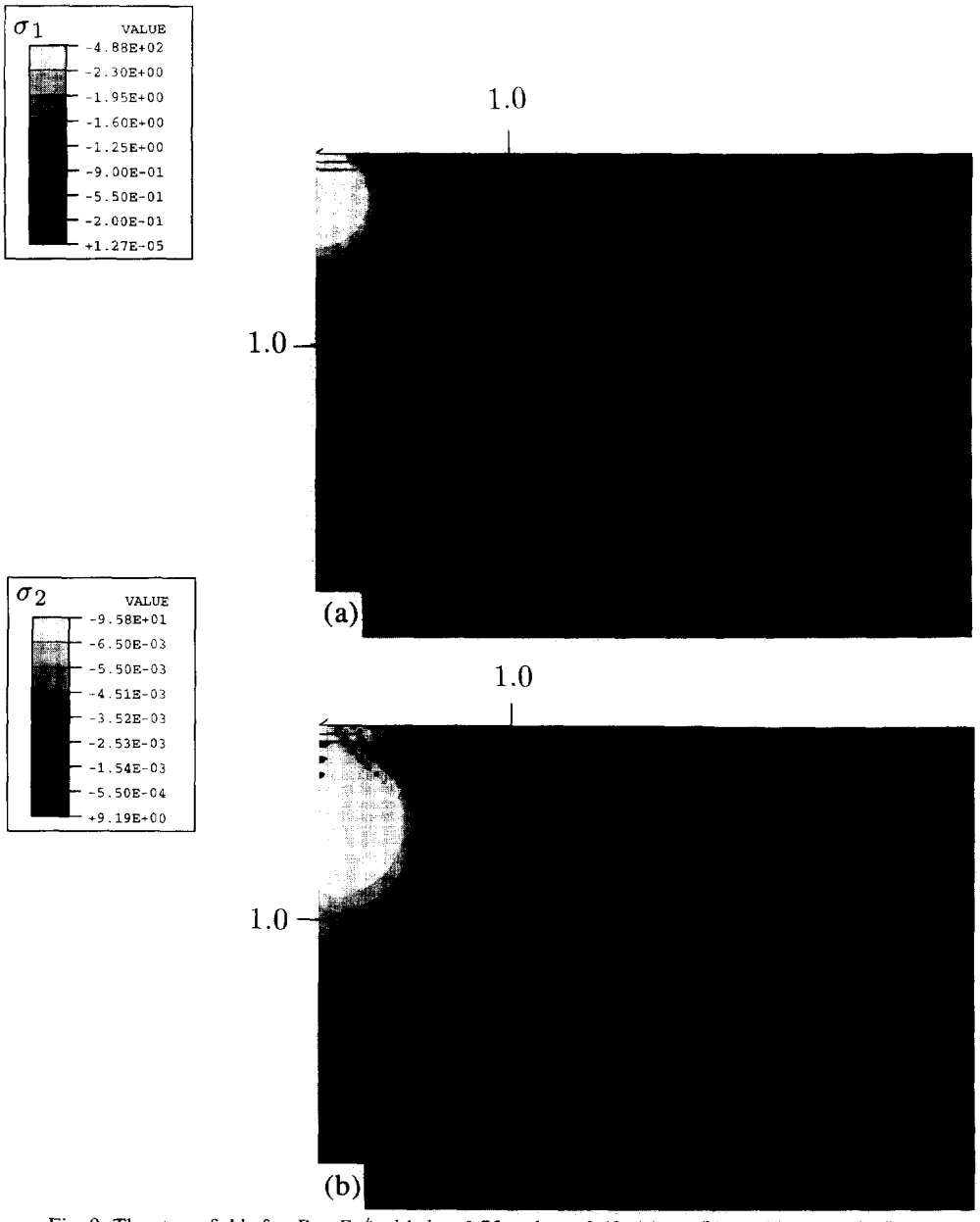

Fig. 9. The stress fields for $E = E_0 z^k$ with $k = 0.75$ and $\nu = 0.43$. (a) σ_1, (b) σ_2, (c) $\sigma_{\theta\theta}$, and (d) σ_{rz} (lengths are in m and stresses in Pa). (*Continued overleaf.*)

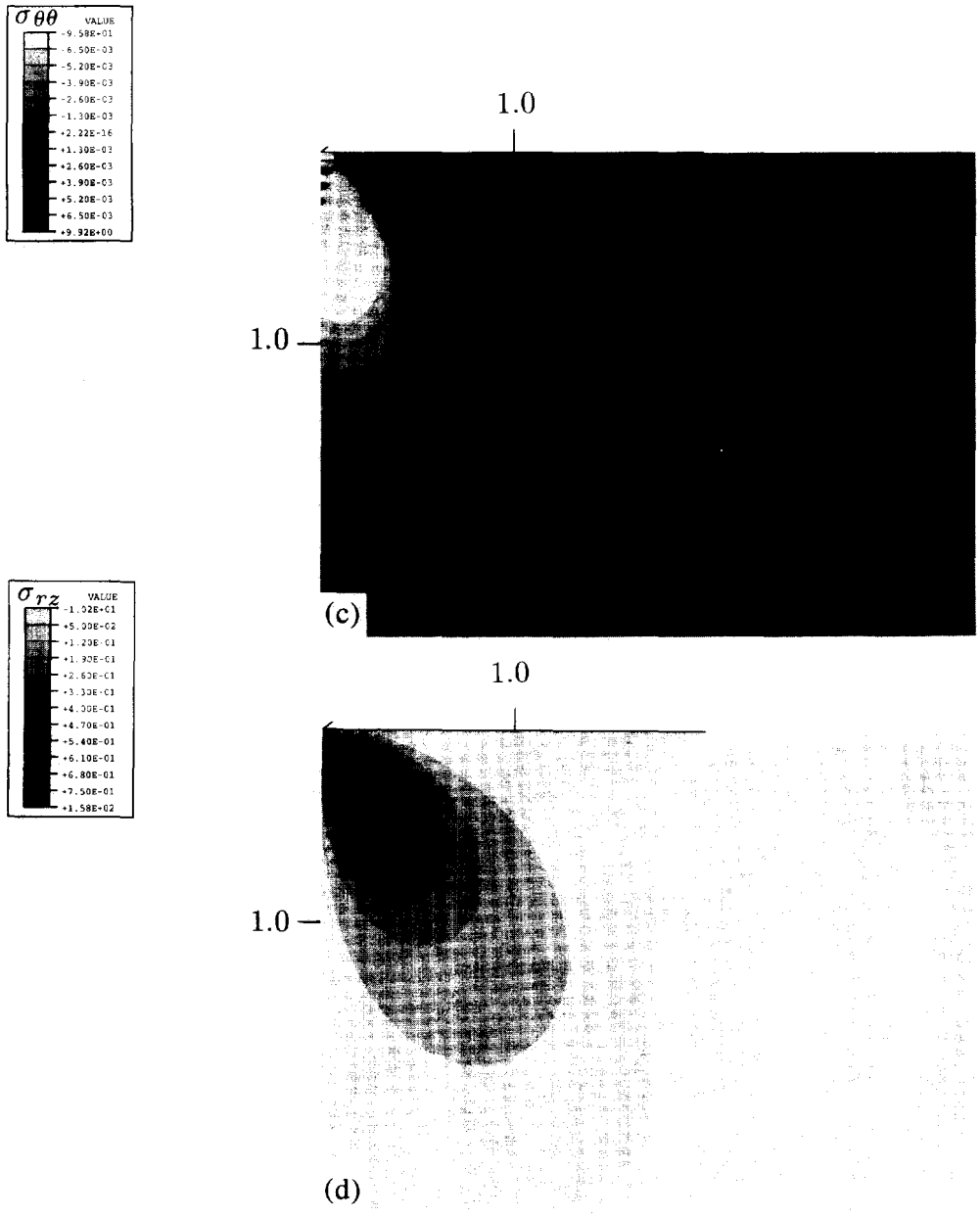

Fig. 9—*Continued.*

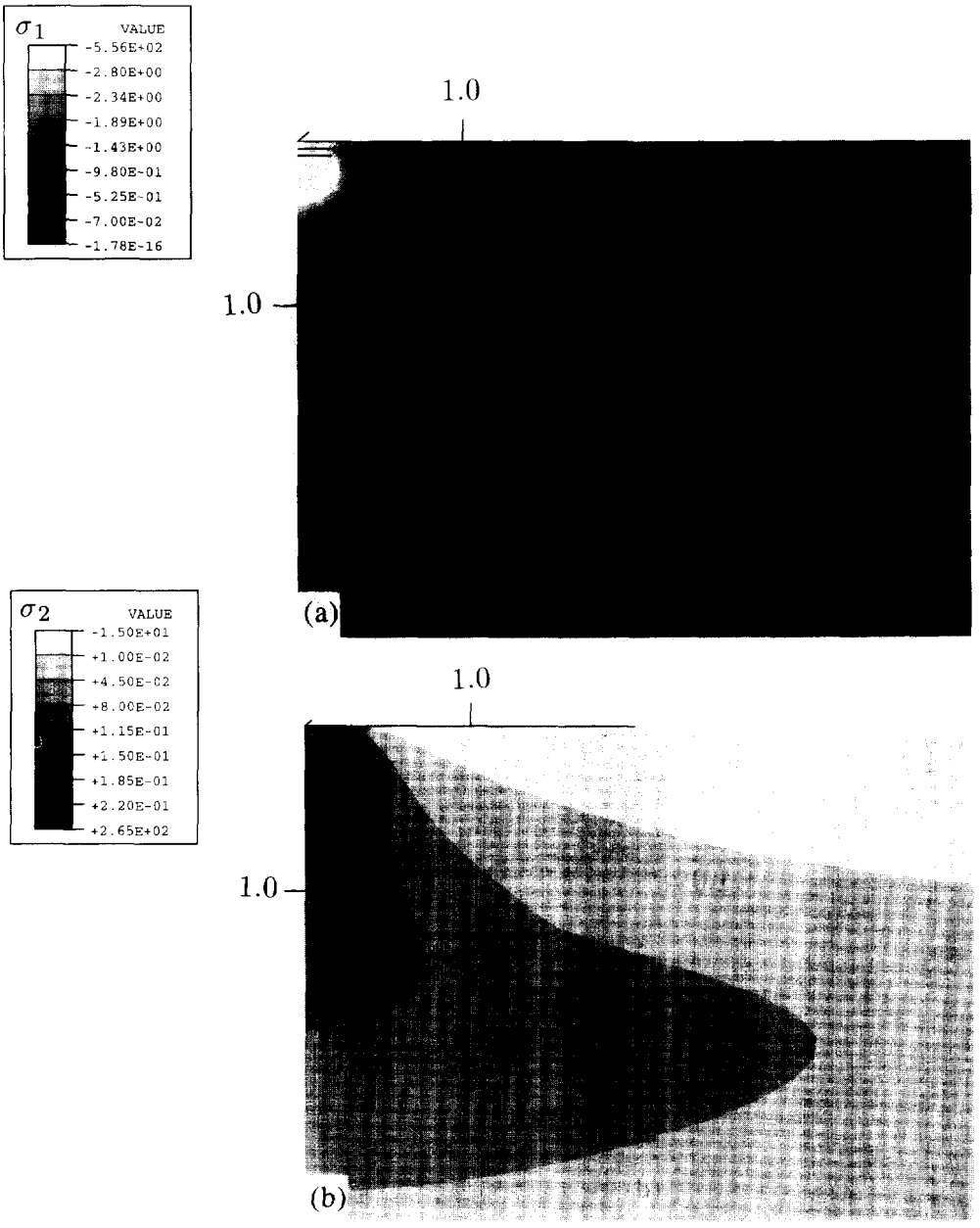

Fig. 10. The stress field for $E = E_0 e^{\alpha z}$ with $\alpha = -1.0$ and $\nu = 0.2$. (a) σ_1, (b) σ_2, (c) $\sigma_{\theta\theta}$, and (d) σ_{rz} (lengths are in m and stresses in Pa). (*Continued overleaf.*)

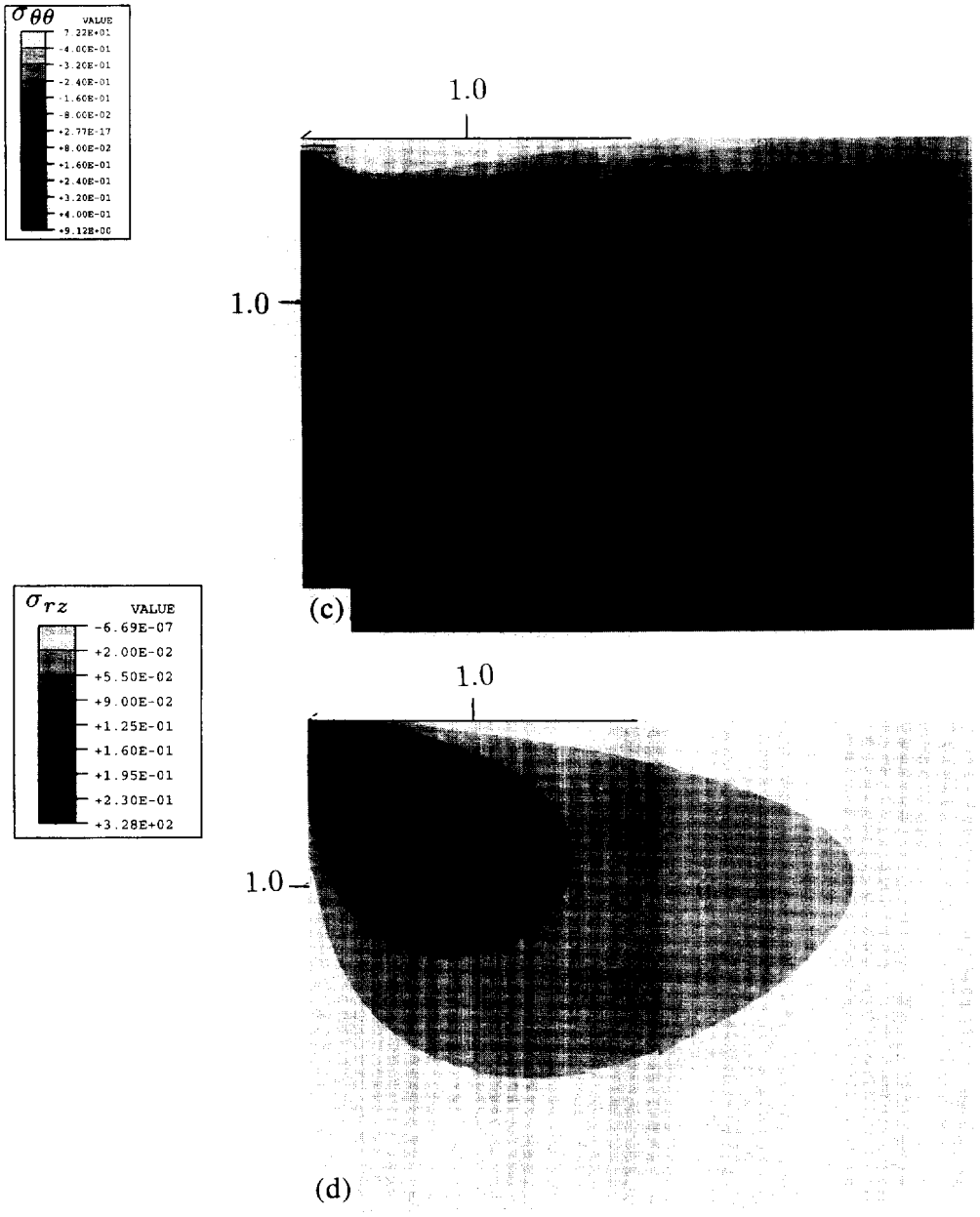

Fig. 10—*Continued.*

from being localized beneath the surface to being spread closer to the surface, as the Poisson ratio increases.

The secondary (smaller in absolute magnitude) principal stress, σ_2, changes sign and varies from being positive (tensile) at $\nu < 1/(k+2)$, to negative (compressive) at $\nu > 1/(k+2)$, and it vanishes at $\nu = 1/(k+2)$. This is of importance for the development of Herzian cone, Palmqvist and lateral cracks at spherical or sharp indentors. A Poisson ratio above the critical value of $1/(k+2)$ may essentially eliminate the deleterious effects of the Hertzian cone type of crack because of the absence of tensile principal stress.

The shear stress field rotates towards the free surface with increasing ν. The angle of maximum shear decreases from around $\phi \approx 52.5°$ at $k = 0$, to $\phi \approx 39°$ at $k = 1$. The same dependence also holds for the $\sigma_{\theta\theta} = 0$ contour. Thus, in good accord with the theory, the location of the $\sigma_{\theta\theta} = 0$ contour coincides with the contour of maximum shear stress σ_{rz}.

In all cases, the dominant principal stress, σ_1, is far larger than the other principal stresses, hence it can with very good accuracy represent the Mises effective stress, or three times the hydrostatic pressure.

4.3. *The exponential law case*: $E = E_0 e^{\alpha z}$

First, we examine the case of $\alpha < 0$. The stresses for a typical case of $\alpha = -1$ and $\nu = 0.2$ are shown in Fig. 10. The Poisson ratio does not markedly influence the stress fields. We note that the coordinates scale inversely with $|\alpha|$, which indicates that the problem is completely defined by ν. As $z \to +\infty$, the stresses approach a biaxial state of compression along the z-axis and tension along the r-axis. The magnitude of the stresses decay exponentially, as predicted by the theory. The secondary principal stress, σ_2, is always tensile. The maximum shear stress, σ_{rz}, follows an exponential curve, as it also decays exponentially with depth, according to $z \approx 1/|\alpha| - 0.084e^{\alpha z}$. The same line is also the contour for the zero circumferential stress ($\sigma_{\theta\theta} = 0$), as expected from the theory. Regarding $\sigma_{\theta\theta}$, it changes sign from tensile (positive) along the z-axis to compressive (negative) close to the surface, as it crosses the zero-value line, $z \approx 1/|\alpha| - 0.084e^{\alpha z}$. Clearly, much more volume of the material experiences tensile stresses than the homogeneous case. Both $\sigma_{\theta\theta}$ and σ_{rz} "sense" the existence of the characteristic length, $1/|\alpha|$, of the problem.

Next, we examine the case of $\alpha > 0$. The stresses for a typical case of $\alpha = 1$ and $\nu = 0.0$, 0.2, 0.4 are shown in Figs 11, 12 and 13, respectively. The Poisson ratio strongly influences the stress fields and, in particular, σ_2 and $\sigma_{\theta\theta}$. The shear stress is directed towards the bulk of the material and remains relatively invariant with α and ν. At low values of ν ($\nu \to 0$), the dominant principal stress, σ_1, is compressive, focuses in the interior. The secondary principal stress, σ_2, is tensile with values lower than those for $\alpha < 0$. The circumferential stress, $\sigma_{\theta\theta}$, is higher than that of the homogeneous case but lower than the $\alpha < 0$ case. The shear stress, σ_{rz}, focuses more to the interior than the homogeneous case. At high values of ν ($\nu \to 0.5$), the dominant principal stress, σ_1, is compressive and resembles that of the homogeneous case. The secondary principal stress, σ_2, is mainly compressive (a maximum compression appears below the surface at a distance of about $2/(3\alpha)$) with a tensile region close to the point force. Table 3 contains the comparisons of the exponential model for $\alpha < 0$, $\alpha > 0$ and $\alpha = 0$ (homogeneous case). As in the power law case, the dominant principal stress, σ_1, is far larger that all other principal stresses, hence it can with very good accuracy represent the Mises effective stress, or three times the hydrostatic pressure.

5. CONCLUSIONS

The present work provides the solutions for the case of a point force compressing normally the surface of an elastic half-space wherein the elastic properties vary with distance normal to the indented surface. Two basic variations of the elastic modulus with depth were examined: the power law ($E = E_0 z^k$) and the exponential law ($E = E_0 e^{\alpha z}$). These models capture the elastic behavior of many geomechanical deposits, as well as of graded structural materials. Analysis and finite elements were used to capture the solution at the surface and in the interior of the half-space. The theory is based on elasticity methods for axisymmetric equilibrium problems and is aimed at obtaining such results as surface

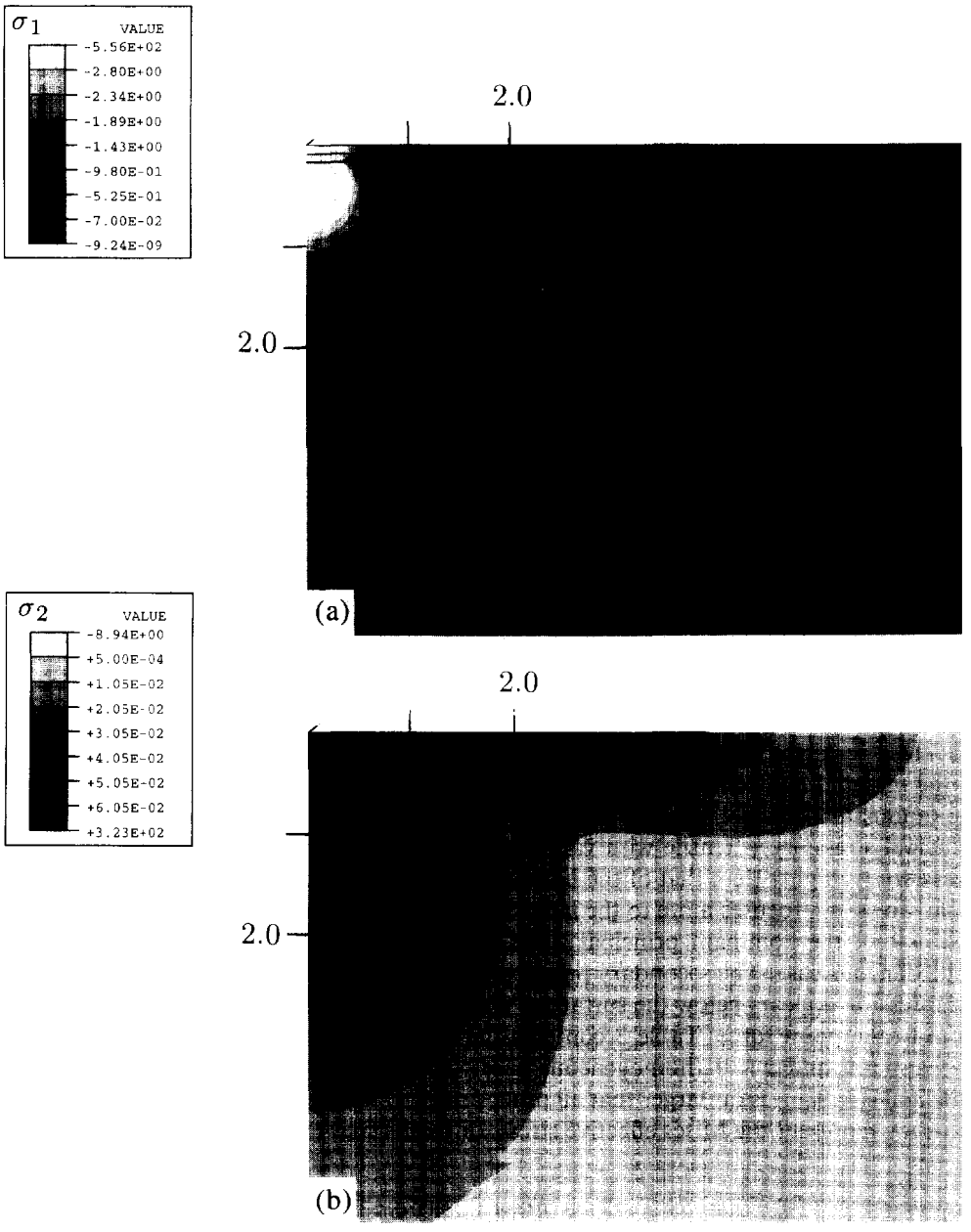

Fig. 11. The stress fields for $E = E_0 e^{\alpha z}$ with $\alpha = 1.0$ and $\nu = 0.0$. (a) σ_1, (b) σ_2, (c) $\sigma_{\theta\theta}$, and (d) σ_{rz}, shear stress (lengths are in m and stresses in Pa). (*Continued opposite.*)

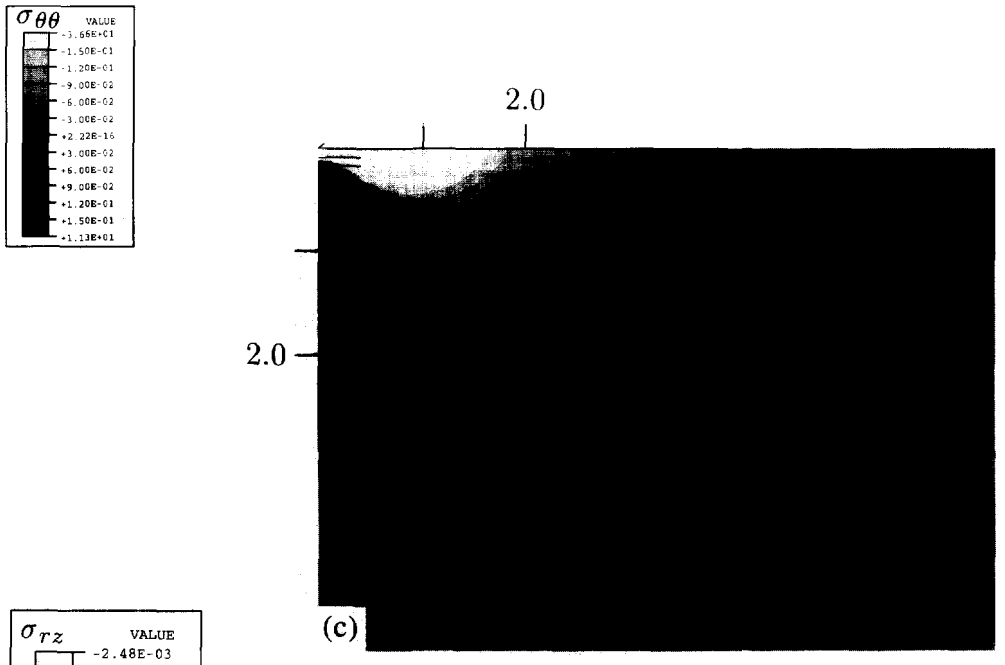

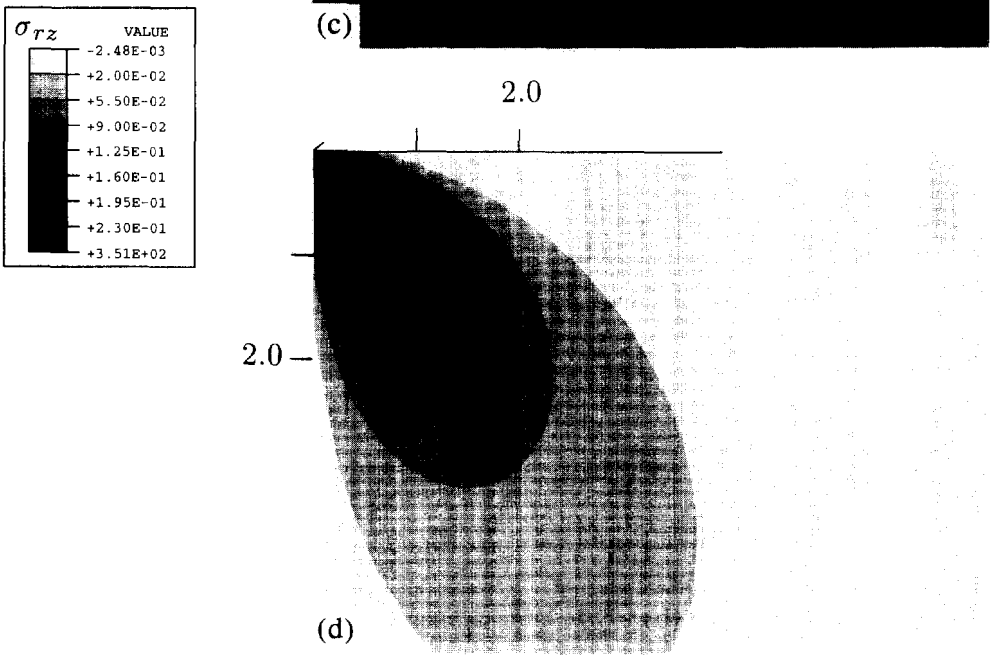

Fig. 11—*Continued.*

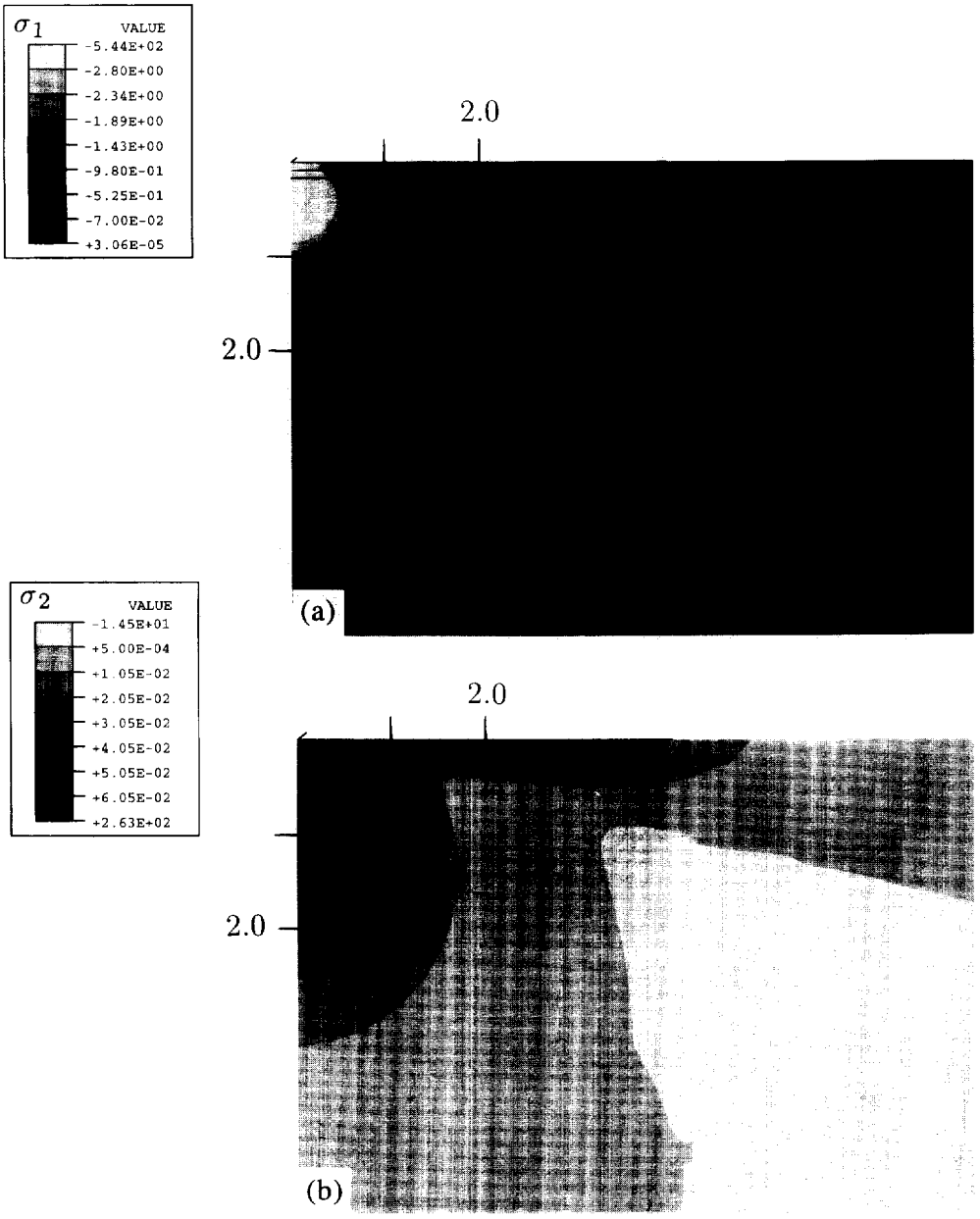

Fig. 12. The stress fields for $E = E_0 e^{\alpha z}$ with $\alpha = 1.0$ and $\nu = 0.2$ (a) σ_1, (b) σ_2, (c) $\sigma_{\theta\theta}$, (d) σ_{rz} (lengths are in m and stresses in Pa). (*Continued opposite.*)

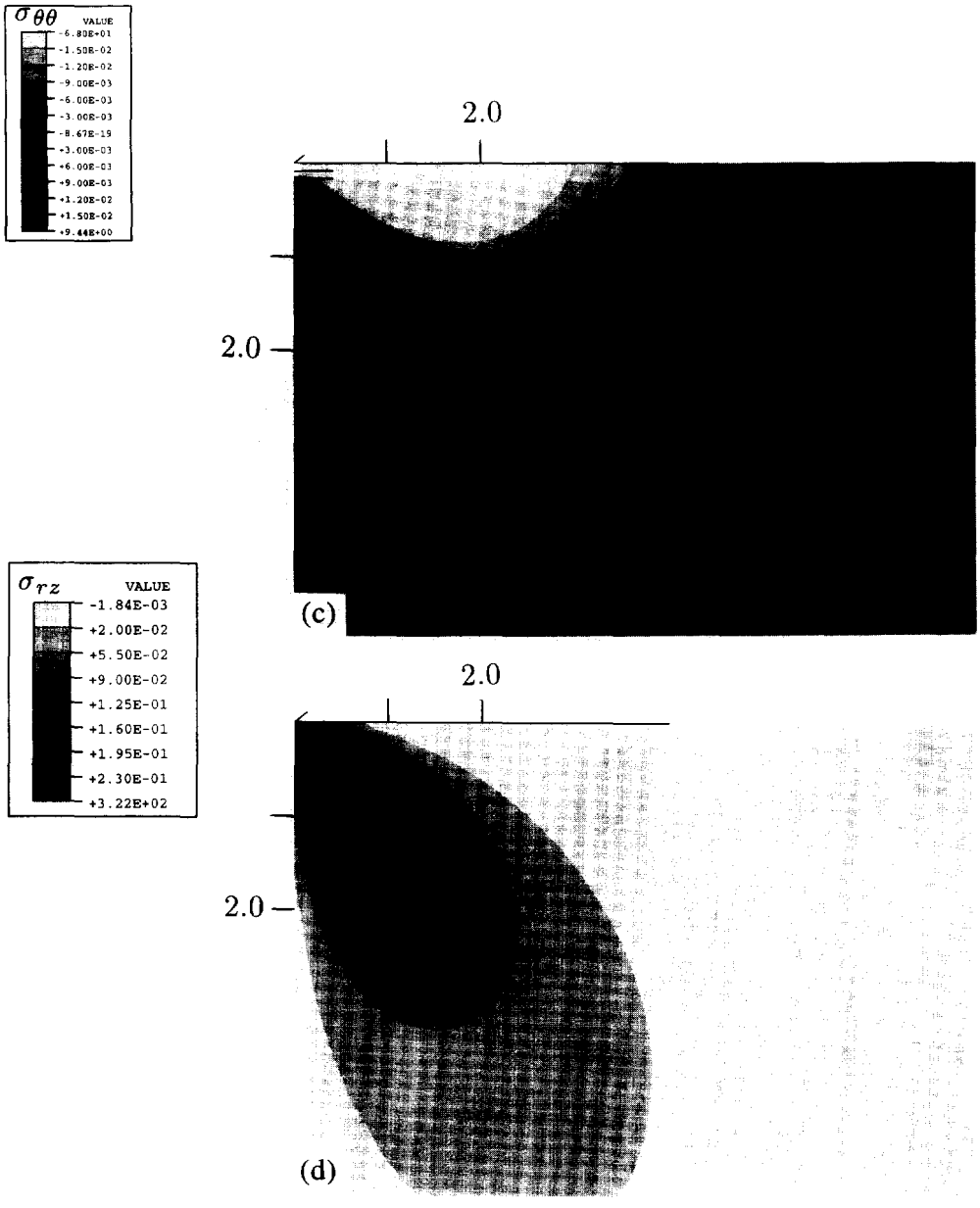

Fig. 12—*Continued.*

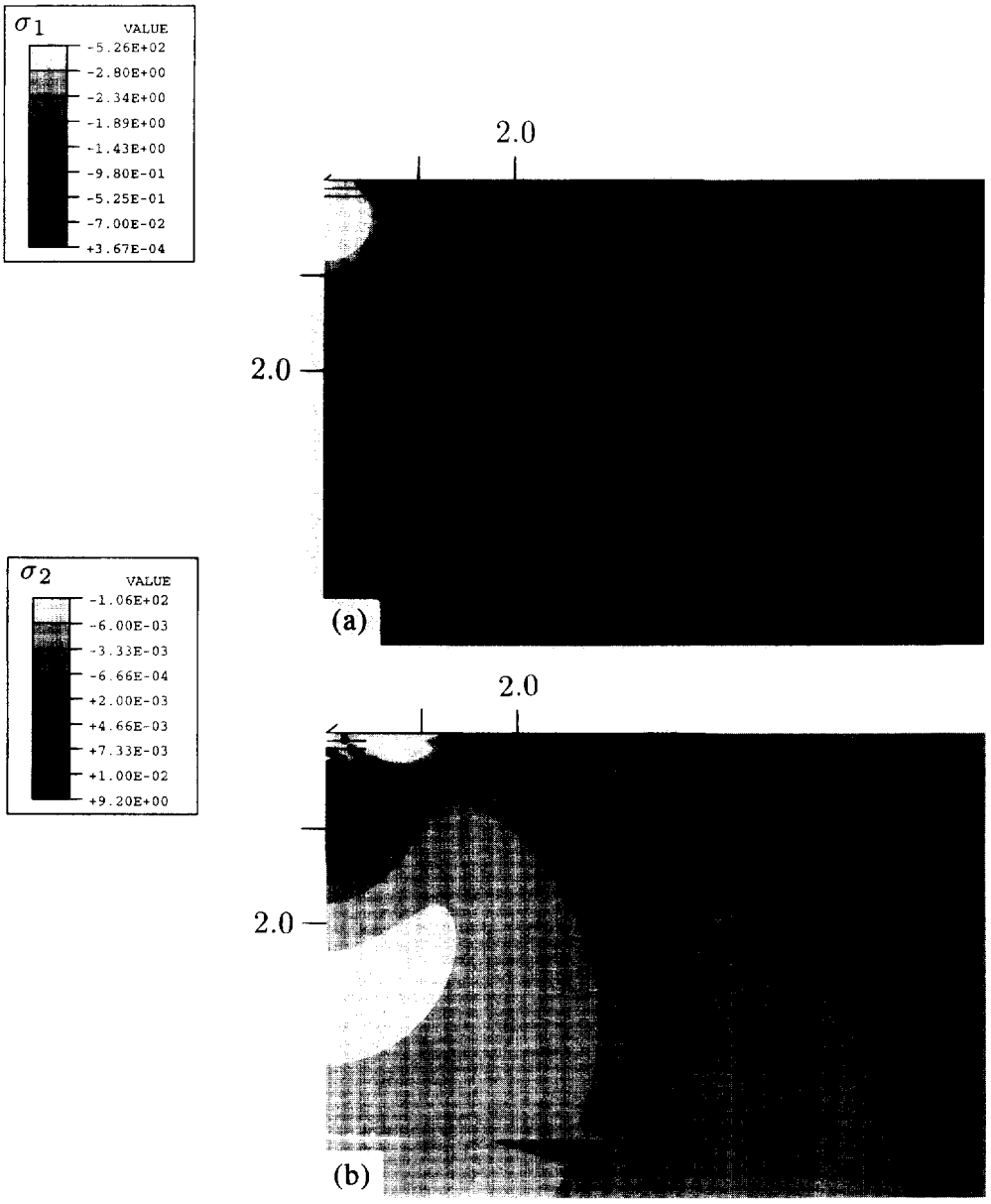

Fig. 13. The stress fields for $E = E_0 e^{\alpha z}$ with $\alpha = 1.0$ and $\nu = 0.4$ (a) σ_1, (b) σ_2, (c) $\sigma_{\theta\theta}$, (d) σ_{rz} (lengths are in m and stresses in Pa). (*Continued opposite.*)

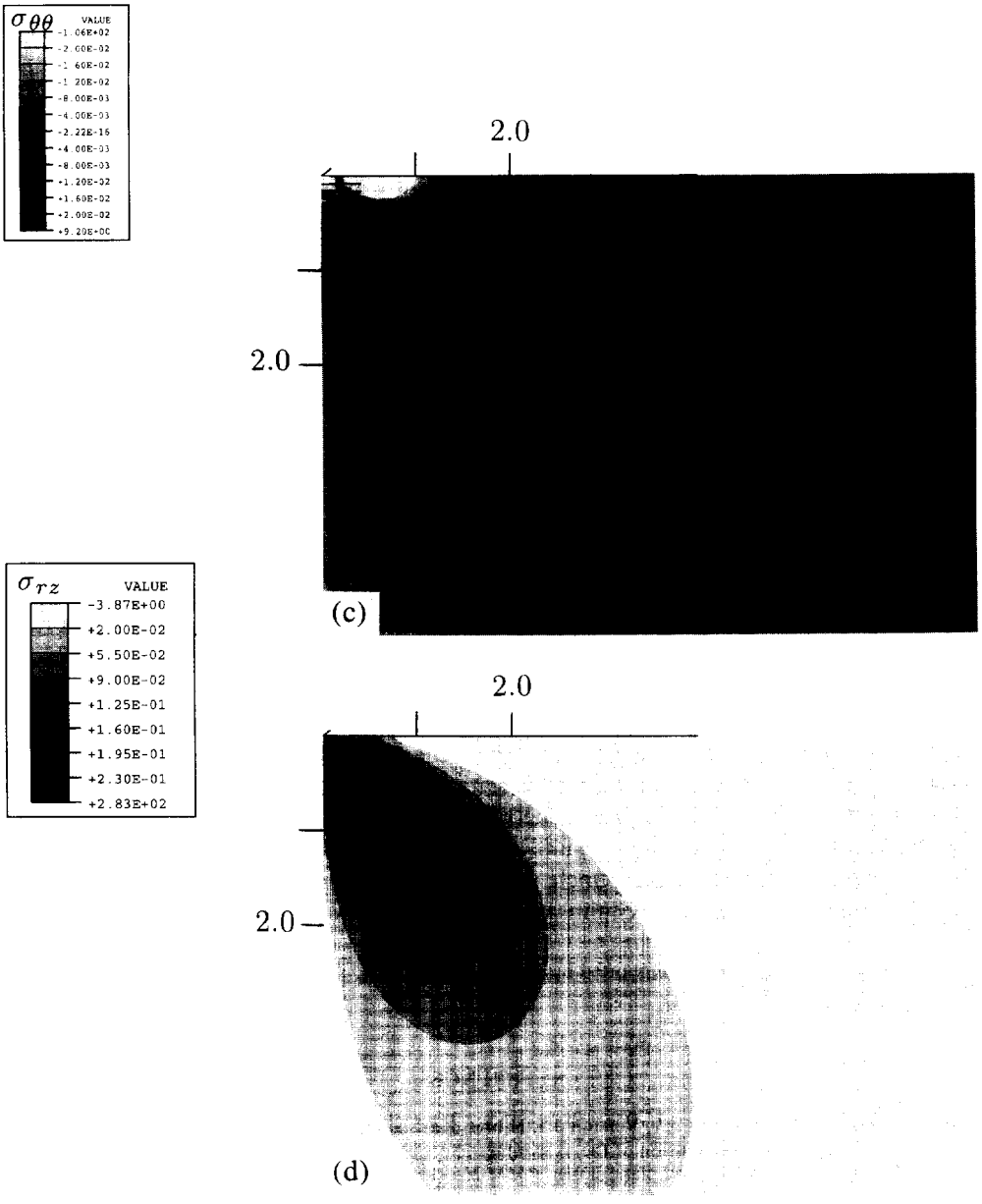

Fig. 13—*Continued.*

deformation and stresses along the line of the applied force. An inhomogeneous-type finite element was developed to capture the continuously (or discontinuously) varying elastic properties. The complete finite element solution revealed some very interesting features in the interior of the half-space that arise from the influence of the Poisson ratio and the rate of change of the elastic modulus.

The influence of the Poisson ratio is strong whenever the elastic modulus is increasing with depth, and is weak whenever the elastic modulus is decreasing with depth. This behavior can be related to the competing constraint between the elastic modulus distribution and the increasing Poisson ratio towards the incompressibility limit ($\nu \to 0.5$).

For the power law model, it was found that there is a critical Poisson ratio ($\nu_{cr} = 1/(k+2)$) which signals drastic changes in the stress fields. For $\nu < \nu_{cr}$, the in-plane dominant principal tensile stress is compressive and the secondary principal stress is tensile. The circumferential stress is tensile in a conical region below the point force and compressive elsewhere. For $\nu = \nu_{cr}$, there is only one principal (compressive) stress acting in the radial direction away from the point force. For $\nu > \nu_{cr}$, both the in-plane principal stresses are compressive. The circumferential stress is compressive in a conical region below the point force and tensile elsewhere. As a result, possible macro- and micro-cracking patterns are expected to be strongly affected by the Poisson ratio, as our punch solutions have indicated (Giannakopoulos and Suresh, 1997). Commencement of plasticity in metal matrix composites, water saturation in soils, and moisture absorption in plastic materials are all factors which additionally influence indentation results, increasing the effective Poisson ratio towards incompressibility; consequently, the solutions for $\nu > \nu_{cr}$ become more relevant.

Regarding the change of the elastic modulus, it was found that a decreasing elastic modulus with depth results in the spreading of stresses towards the surface rather than to the interior, whereas an increasing elastic modulus results in diffusing the stresses towards the interior of the half-space. In all cases the load diffusion is far smoother for the graded material than for sharp layered cases (e.g., films on substrate), thus avoiding severe stress jumps that may promote delaminations or other forms of damage. On the other hand, a decreasing elastic modulus with depth results in a large surface deformation which is less localized than the surface deformation for increasing elastic modulus. The above results are of importance in indentation and penetration analysis, and for surface engineering with coatings for structural components. They show that graded materials can be tailored (in this case, by appropriately modifying the variation of elastic properties with depth) to meet specific requirements of tribological, penetration and foundation problems in mechanical and civil engineering. The present results also provide the basic formulations upon which our subsequent analyses of the punch, spherical and conical indentation problems for graded materials are predicted (Giannakopoulos and Suresh, 1997).

Acknowledgements—This work was supported by the U.S. Office of Naval Research under Grant N-00014-94-1-0139 to MIT.

REFERENCES

ABAQUS (1993). *Finite Element Code*, Version 5.3, Hibbit, Karlsson and Sorenson, Inc., Providence, RI.

Aleksandrov, A. I. (1961). The solution of the axisymmetric problem of the theory of elasticity with the aid of a relation between axisymmetric and plane states. *PMM* **25,** 912–920.

Awojobi, A. O. and Gibson, R. E. (1973). Plane strain and axially symmetric problems of a linearly non-homogeneous elastic half-space. *Quarterly Journal of Mechanics and Applied Mathematics* **26,** 285–302.

Bell, F. G., Culshaw, M. G., Cripps, J. C. and Coffey, J. R. (eds) (1990). *Field testing in Engineering Geology*, Geological Society, Engineering Geology Special Publication No. 6.

Booker, J. R., Balaam, N. P. and Davis, E. H. (1985). The behaviour of an elastic non-homogeneous half-space. Part I—Line and point loads. *International Journal of Numerical and Analytical Methods in Geomechanics* **9,** 353–367.

Boussinesq, M. J. (1885). *Application Des Potentials, a l'Etude de l'Equilibre et du Mouvement Des Solides Elastiques*, Gauthier-Villars, Paris.

Brown, P. T. and Gibson, R. E. (1972). Surface settlement of a deep elastic stratum whose modulus increases linearly with depth. *Canadian Geotechnology Journal* **9,** 467–476.

Calladine, C. R. and Greenwood, J. A. (1978). Line and point loads on a non-homogeneous incompressible elastic half-space. *Quarterly Journal of Mechanics and Applied Mathematics* **31,** 507–529.

Ching-Hua, D. (1961). The two-dimensional problems of the non-homogeneous isotropic medium. In *Problems of Continuum Mechanics*, Akad. Naukk SSSR, pp. 104–108.
Dowding, C. H. (ed.) (1978). *Site Characterization and Exploration*, ASCE, NY.
Finot, M., Suresh, S., Bull, C., Giannakopoulos, A. E., Olsson, M. and Sampath, S. (1994). Experimental studies of thermal cycling of a Ni-Al_2O_3 graded material. In *3rd Int. Symp. on Structural and Functional Gradient Materials*. Lausanne, Switzerland, (eds Ilschner, B. and Cherradi, N.), pp. 229–234.
Fitzgerald, E. A., Xie, Y.-H., Monroe, D., Silverman, P. J., Kuo, J.-M., Kortan, A. R., Thiel, F. A., Weir, B. E. and Feldman, L. C. (1992). Relaxed Ge_xSi_{1-x} structures for III-V integration with Si and high mobility two-dimensional electron gases in Si and high mobility two-dimensional electron gases in Si. *Journal of Vacuum Science and Technology* **B10,** 1807–1819.
Giannakopoulos, A. E., Suresh, S., Finot, M. and Olsson, M. (1995). Elastoplastic analysis of thermal cycling: Layered materials with compositional gradients. *Acta Metallurgica and Materials* **43,** 1335–1354.
Giannakopoulos, A. E. and Suresh, S. (1997). Indentation of solids with gradients in elastic properties: Part II. Axisymmetric indentors. *International Journal of Solids and Structures*, **34,** 2393–2428.
Gibson, R. E. (1967). Some results concerning displacements and stresses in a non-homogeneous elastic half-space. *Geotechnique* **17,** 58–67.
Gibson, R. E., Brown, P. T. and Andrew, K. R. F. (1971). Some results concerning displacements in a non-homogeneous elastic layer. *ZAMP* **22,** 855–864.
Gibson, R. E. and Kalsi, G. S. (1974). The surface settlement of a linearly inhomogeneous cross-anisotropic elastic half-space. *ZAMP* **25,** 843–847.
Gibson, R. E. and Sills, G. C. (1975). Settlement of a strip load on a non-homogeneous orthotropic incompressible elastic half-space. *Quarterly Journal of Mechanics and Applied Mathematics* **28,** 233–243.
Gladwell, G. M. L. (1980). *Contact Problems in the Classical Theory of Elasticity*, Sijthoff and Noordhoff, Netherlands.
Hills, P. A., Nowell, D. and Sackfield, A. (1993). *Mechanics of Elastic Contacts*, Butterworth-Heineman Ltd.
Holl, D. L. (1940). Stress transmission in earths. *Proceedings of the High Research Board* **20,** 709–721.
Hruban, K. (1958). The basic problem of a non-linear and non-homogeneous half-space. In *Non-homogeneity in Elasticity and Plasticity IUTAM Symp.*, Warsaw, Pergamon Press, pp. 53–61.
Ilschner, B. and Cherradi, N. (eds.) (1994). *3rd Int. Symp. on Structural and Functional Gradient Materials*, Lausanne, Switzerland.
Johnson, K. L. (1985). *Contact Mechanics*, Cambridge University Press, Cambridge.
Judd, W. (ed) (1964). *State of Stress in the Earth's Crust*, Santa Monica, CA.
Kezdi, A. and Lazanyi, I. (eds.) (1976). *Proc. 5th Budapest Conf. on Soil Mechanics and Foundation Engng*, Budapest.
Lekhnitskii, S. G. (1962). Radial distribution of stresses in a wedge and in a half-plane with variable modulus of elasticity. *PMM* **26,** 146–151.
Love, A. E. H. (1927). *A Treatise on the Mathematical Theory of Elasticity*, 4th ed., Cambridge.
Magnus, W. and Oberhettinger, F. (1954). *Formulas and Theorems for the Functions of Mathematical Physics*. Chelsea Publ. Co. N.Y.
Mossakovskii, V. I. (1958). The pressure of a circular stamp on an elastic half space whose modulus of elasticity is a power function of depth. *PMM* **22,** 123–125.
O'Neill, M. W. and Dobry, R. (eds.) (1980). *Dynamic Response of Pile Foundations: Analytical Aspects*, ASCE, NY.
Pariseau, W. G. (ed.) (1984). *Geomechanics Applications in Underground Hardrock Mining*, Soc. Mining Engng, N.Y.
Pells, P. J. N. (ed.) (1985). *Engineering Geology of the Sydney Region*, Australian Geomechanics Society, A. A. Balkerna Publ.
Prakash, S. (ed.) (1984). *Int. Conf. on Case Histories in Geotechnical Engineering*, vol. I, Univ. of Missuri-Rolla, U.S.A.
Rostovtsev, N. A. and Khranevskaia (1971). The solution of the Boussinesq problem for a half-space whose modulus of elasticity is a power function of the depth. *PMM* **35,** 1053–1061.
Suresh, S. and Needleman, A. (eds) (1996). Mechanics and physics of layered and graded materials. *Journal of Mechanics, Physics and Solids* **44**(5), special issue.
Whittaker, E. T. and Watson, G. N. (1962). *A Course of Modern Analysis*. Cambridge University Press, Cambridge, U.K.

APPENDIX 1: THE BOUSSINESQ SOLUTION

Bousinesq (1885) found the solution for a point force of magnitude P directed in a homogeneous, elastic, isotropic half space, $z \geqslant 0$, under small strain formulation. Taking a cylindrical coordinate system (r, z, θ) at the point of the applied force, the non-zero stresses are

$$\sigma_{zz} = -\frac{3P}{2\pi}\frac{z^3}{R^5}$$

for the vertical stress ($R^2 = z^2 + r^2$),

$$\sigma_{rr} = -\frac{P}{2\pi}\left(\frac{3zr^2}{R^5} - \frac{1-2v}{R(R+z)}\right)$$

for the radial stress,

$$\sigma_{\theta\theta} = -\frac{P(1-2\nu)}{2\pi}\left(\frac{1}{R(R+z)} - \frac{z}{R^3}\right)$$

for the circumferential stress and

$$\sigma_{rz} = \frac{3P}{2\pi}\frac{z^2 r}{R^5}$$

for the shear stress.

APPENDIX 2: THE GENERAL SOLUTION OF THE SURFACE DISPLACEMENT IN THE EXPONENTIAL MODEL

The influence function for the exponential model is given by the surface displacement of a point load P

$$w(r) = \frac{1}{4\pi m E_0}\int_0^\infty q\frac{g_1}{g_2}J_0(qr)\,\mathrm{d}q$$

where J_0 is the Bessel function of the first kind, of zeroth order,

$$m = \frac{1}{2(1+\nu)}, \quad n = \frac{\nu}{(1+\nu)(1-2\nu)}, \quad \gamma^2 = \frac{n}{2m+n}$$

$$a_q^2 = \tfrac{1}{8}(\sqrt{(\alpha^2+4q^2)^2+(4\alpha\gamma q)^2}+(\alpha^2+4q^2))$$

$$b_q^2 = \tfrac{1}{2}(\sqrt{(\alpha^2+4q^2)^2+(4\alpha\gamma q)^2}-(\alpha^2+4q^2))$$

$$g_1 = 2(1-\nu)(a_q+\alpha/2)q^2-(1-\nu)(1-2\nu)\alpha q^2+(1-2\nu)\nu\alpha((a_q+\alpha/2)^2+b_q^2)$$

$$g_2 = \nu(1-\nu)((a_q+\alpha/2)^2+b_q^2)^2+((1-\nu)^2(3(a_q+\alpha/2)^2-b_q^2)+(2-\nu)\nu((a_q+\alpha/2)^2+b_q^2)$$
$$-2(1-\nu)\alpha(a_q+\alpha/2))q^2-(1-\nu)(2-\nu)q^4.$$